INFORMATION TO USERS

This manuscript has been reproduced from the microfilm master. UMI films the text directly from the original or copy submitted. Thus, some thesis and dissertation copies are in typewriter face, while others may be from any type of computer printer.

The quality of this reproduction is dependent upon the quality of the copy submitted. Broken or indistinct print, colored or poor quality illustrations and photographs, print bleedthrough, substandard margins, and improper alignment can adversely affect reproduction.

In the unlikely event that the author did not send UMI a complete manuscript and there are missing pages, these will be noted. Also, if unauthorized copyright material had to be removed, a note will indicate the deletion.

Oversize materials (e.g., maps, drawings, charts) are reproduced by sectioning the original, beginning at the upper left-hand corner and continuing from left to right in equal sections with small overlaps. Each original is also photographed in one exposure and is included in reduced form at the back of the book.

Photographs included in the original manuscript have been reproduced xerographically in this copy. Higher quality 6" x 9" black and white photographic prints are available for any photographs or illustrations appearing in this copy for an additional charge. Contact UMI directly to order.

UMI

University Microfilms International
A Bell & Howell Information Company
300 North Zeeb Road, Ann Arbor, MI 48106-1346 USA
313/761-4700 800/521-0600

Order Number 1349477

Numerical model for calculating the ultrasonic power deposition in layered medium

Fan, Xiaobing, M.S.

The University of Arizona, 1992

U·M·I
300 N. Zeeb Rd.
Ann Arbor, MI 48106

NUMERICAL MODEL FOR CALCULATING THE ULTRASONIC POWER DEPOSITION IN LAYERED MEDIUM

by

Xiaobing Fan

A Thesis Submitted to the Faculty of the

Department of Electrical and Computer Engineering

In Partial Fulfillment of the Requirements
For the Degree of

MASTER OF SCIENCES
WITH A MAJOR IN ELECTRICAL ENGINEERING

In the Graduate College

THE UNIVERSITY OF ARIZONA

1992

STATEMENT BY AUTHOR

This thesis has been submitted in partial fulfillment of requirements for an advanced degree at The University of Arizona and is deposited in the University Library to be made available to borrowers under rules of the library.

Brief quotations from this thesis are allowable without special permission, provided that accurate acknowledgement of source is made. Requests for permission for extended quotation from or reproduction of this manuscript in whole or in part may be granted by the head of the major department or the Dean of the Graduate College when in his or her judgment the proposed use of the material is in the interests of scholarship. In all other instances, however, permission must be obtained from the author.

SIGNED: Xiaobing Jan

APPROVAL BY THESIS DIRECTOR

his thesis has been approved on the date shown below:

Hal S. Tharp

Hal S. Tharp
Assistant Professor of
Electrical and Computer Engineering

7/28/92

Date

ACKNOWLEDGMENTS

The author would like to express sincere thanks to Dr. Kullervo Hynynen, Dr. Robert Roemer and Dr. Hal Tharp for their constant advice, guidance and encouragement during this project. Special thanks to the following colleagues: Dennis Anhalt, Mark Buchannan, Andy Dutton, Scott Nathanson, and Matt Rademacher who provided friendship, technical support and advice for this work. He would also like to offer thanks to Dr. Andreas Cangellaris and Dr. David Lomen.

The author would like to express his most sincere thanks to his parents, Zhiying Cheng and his departed father Zhangwu Fan, for all of their love and encouragement. The author offers his appreciation to his wife, Yixia Lu, his daughter, Lisa Fan, his mother-in-law, Aizhen Li, his uncle, Changyun Fan and his aunt, Zongying Deng for their love, support and encouragement.

This research was supported by NCI grant CA 33922.

TABLE OF CONTENTS

TABLE OF CONTENTS - continued

LIST OF FIGURES

LIST OF FIGURES - continued

LIST OF TABLES

ABSTRACT

An improved numerical model for calculating the ultrasonic power deposition in layered medium was developed and experimentally verified. The new model takes into account the ultrasound wave reflection and refraction at irregular tissue interfaces thereby providing improved accuracy in ultrasound hyperthermia treatment planning. The model was compared with a simplified model to evaluate when the tissue interfaces could be ignored in the hyperthermia treatment planning and evaluation. The effects of variations in water and tissue temperatures, the fat layer thicknesses, the bone-tissue interface, and the beam entrance angles were also investigated to establish guidelines for treatment execution. It was found that in most cases the effects of the soft tissue interfaces can be ignored. However, in some instances the acoustic focus may be shifted several millimeters off axis in layered medium. This is important when sharply focused transducers are used for ultrasound surgery or under the condition of pulsed, high temperature hyperthermia treatments.

CHAPTER 1

1. INTRODUCTION

For ultrasound hyperthermia treatments of tumors (Lele 1983) and also for determining the safety limits of diagnostic ultrasound equipment (AIUM 1988) it is very important to be able to calculate the ultrasound field distribution accurately in tissue. For hyperthermia studies the pressure fields have usually been calculated by evaluating the Rayleigh-Sommerfeld diffraction integral over the surface of a radiator for each field point of interest. To simplify and speed up the calculations, the soft tissues have been simulated as a homogeneous, uniformly attenuating medium (for example Lele and Parker 1982, Hynynen *et al.*, 1981, Swindell *et al.*, 1982, Roemer *et al.*, 1984, Cain and Umemura 1986, Moros *et al.*, 1988, 1990, Diederich and Hynynen 1989, 1990, Lin *et al.*, 1990). Since the impedances of different soft tissues are very close, the sound wave reflection and refraction have been ignored at the tissue interfaces when calculating the acoustic power in tissue. Recently, however, with the use of large aperture, sharply focussed and multiple ultrasound fields to treat deep tumors (Lele 1989, Hynynen *et al.*, 1990) these interfaces have become more important. It has also been proposed that by using sharply focussed ultrasound fields at high power levels a small tissue volume could be treated with a short ultrasound pulse. The temperature elevation during a few second exposure is almost independent of the tissue perfusion which is the main uncertainty in the temperature calculations. Thus, it may be possible

to calculate the temperature elevation and eliminate the need of invasive temperature measurements during these treatments (Billard *et al.*, 1989, 1990, Davis and Lele 1989). This requires that the ultrasound field distribution and the location of the focus be accurately predicted. For these reasons the effects of wave reflection and refraction at the soft tissue interfaces need to be studied, and improved numerical models need to be developed that can provide the required information for treatment planning in ultrasound hyperthermia. This thesis describes an ultrasound beam calculation model that takes beam reflection and refraction into account at tissue interfaces. After the model is tested experimentally it is used to investigate the effects of various soft tissue layers on strongly focussed ultrasound fields. The model is then compared with a simplified model (Swindell *et al.*, 1982) to evaluate when the tissue interfaces can be ignored in the treatment planning and evaluation. The results should also show the accuracy of the system when used in design and optimization studies which until now have assumed uniform acoustic properties throughout the whole target volume (for example Lele and Parker 1982, Hynynen *et al.*, 1981, Swindell *et al.*, 1982, Roemer *et al.*, 1984, Moros *et al.*, 1988, 1990, Diederich and Hynynen 1989, 1990, Lin *et al.*, 1990). The effects of variation in water and tissue temperatures, the fat layer thickness, the bone-tissue interface, and the beam entrance angles on the acoustic field are also investigated to establish guidelines for treatment execution.

CHAPTER 2

2. ACOUSTIC FIELD CALCULATION

An approximate theory for acoustic field calculation has been derived for a concave spherical radiator in a non-absorbing medium (O'Neil 1949). The complex velocity potential is given by the Rayleigh-Sommerfeld diffraction integral

$$\psi(r) = \frac{1}{2\pi} \iint_S v_s \frac{e^{-ikr}}{r} ds, \tag{1}$$

where $k = \omega/c = 2\pi/\lambda$ is the wave number, λ is the wave length, ω is the angular frequency, c is the velocity of propagation, r is the distance from the point source on the radiator to the field point, S is the area of the radiator, ds is the source element area, $i = \sqrt{-1}$, and $v_s = v_0 e^{i\omega t}$ is the normal particle velocity on ds (Figure 1). Acoustic pressure at the point of interest P is given by

$$p(r) = \rho \partial\psi/\partial t = i\omega\rho\psi = ikZ\psi, \tag{2}$$

where ρ is the density and $Z = \rho c$ is the acoustic impedance of the medium. Because there is no analytical solution for equation (1), numerical methods must be used. There are three numerical models that have been developed to evaluate equation (1).

2.1 Simplified model

The traditional way of performing this integral is to use two-dimensional summation over the face of the radiator. The rapid phase variation of the e^{-ikr} term forces the summation increments to be very small with correspondingly long

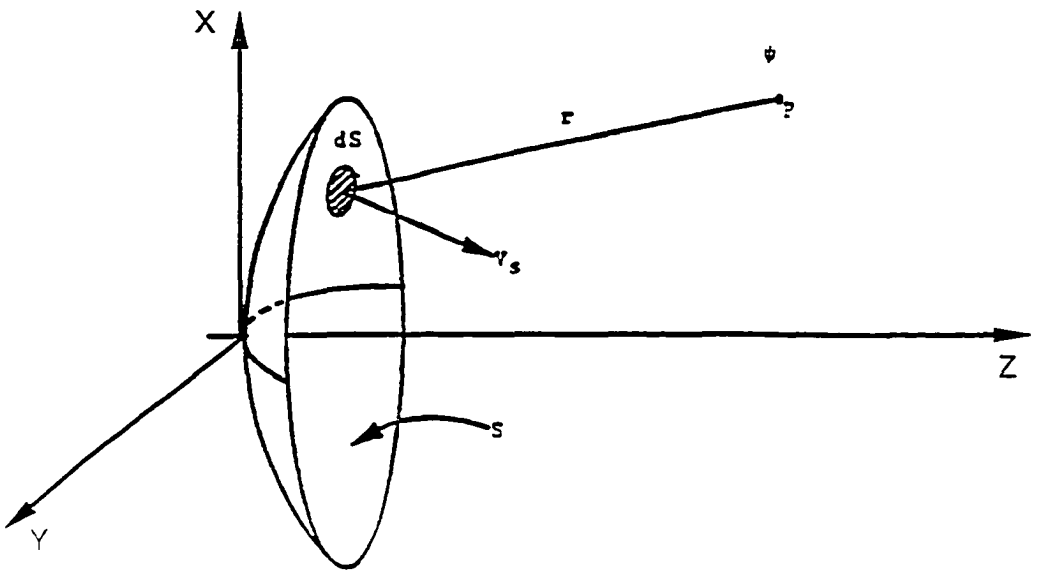

Figure 1. Diagram of the transducer in a medium with regard to a Cartesian coordinate system. The origin of coordinates is at the center of curvature and the z axis is perpendicular to the face of the transducer.

computation times. The essence of the simplified model is to reduce the two-dimensional integral to a one-dimensional integration by considering those elements of area on the transducer over which r is essentially constant. These elements are annular strips centered on the pedal projection of the field point onto the plane of the transducer (Figure 2).

In a weakly attenuating medium, the effect of attenuation can be approximated by $e^{-\alpha r'}$ with r' being the path length in the tissue and α being the linear amplitude attenuation coefficient. In order to speed up the calculations, all of the attenuation ray paths r' can be assumed the same and equal to the normal depth from the interface of water-tissue to the point of interest in the tissue (Swindell *et al.*, 1982). This assumption, which is true for a planar transducer, is a good approximation for a high f-number transducer, but not for a low f-number transducer (f-number = radius of curvature of transducer/diameter of transducer). The simplification allows the double integration in equation (1) to be reduced to a single integration to calculate the acoustic pressure distribution for a continuous wave ultrasound transducer (Madsen *et al.*, 1981,Swindell *et al.*, 1982). The integral can then be approximated by

$$\psi(r) = \frac{1}{2\pi} v_s e^{-\alpha r'} \sum_{m=1}^{M} \frac{e^{-ikr_m}}{r_m} A_m, \tag{3}$$

where A_m is the area of m's annular strip. The total number of annular strips, M, varies depending upon the location of the field point. This water-tissue model can be described as a two layered media with a flat interface parallel to the face of the transducer. The single integration method is fast; however, the effects of discontinuities when the wave travels through interfaces are not considered.

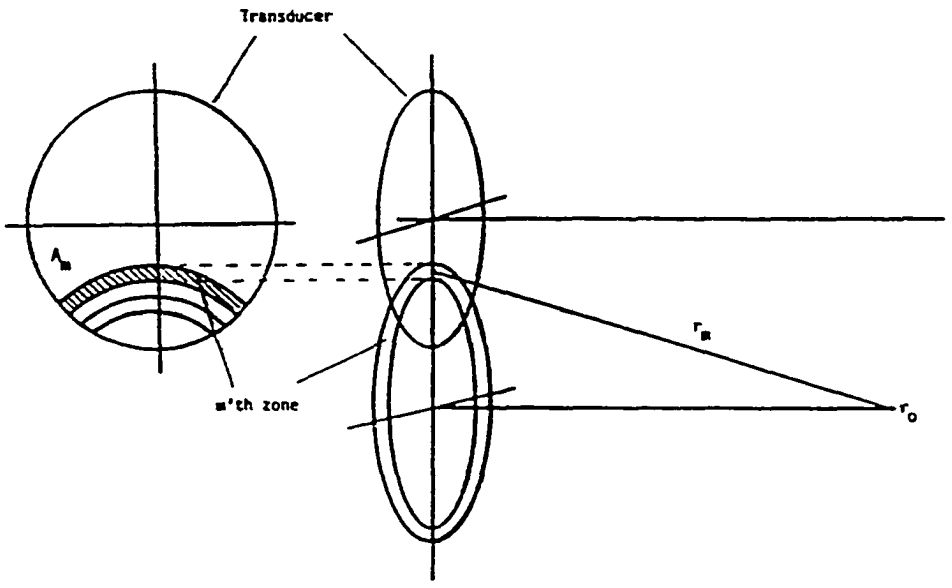

Figure 2. Annular sections of area A_m used in simplified model (illustrated for a planar transducer for clarity).

2.2 Parallel flat plane interface model

In this section, geometrical acoustic theory, ray paths, are used to develop the parallel flat plane interface model. The acoustic pressure field from a point source below the interface of a layered medium can be calculated by multiplying the pressure transmission coefficient and the amplitude diminution factor to the acoustic pressure in the first medium. The incidence angle of the ray was uniquely determined by the velocities of sound, the thickness of each layer and the distance between the point source and the field of interest along the interface direction. The ray path lengths, transmission coefficients and amplitude-diminution factor can be computed from the incidence angles.

When sound waves travel through a medium, they may be reflected or refracted. Refraction of sound waves occurs when a sound wave arrives at a discontinuity or boundary. Some energy crosses the boundary to form transmitted waves and the rest is reflected. Snell's law, applied to the acoustic case in Figure 3, is

$$\frac{\sin(\theta_i)}{c_1} = \frac{\sin(\theta_t)}{c_2} = \frac{\sin(\theta_r)}{c_1}, \tag{4}$$

where c_1 and c_2 are sound velocity in medium 1 and 2; θ_i, θ_r, and θ_t are the angles of incident, reflection, and transmission, respectively, referenced to the normal of the interface of the medium. The pressure field from a point source below the interface of a two layered medium has been studied by Hudimac (1957), Urick (1972) and Young (1973). To show the sound wave reflection and refraction, consider a two layered medium with sound velocity c_i, density ρ_i, and ray path $r_i = H_i/\cos(\theta_i)$ in medium $i = 1, 2$. A point source is located in the first medium, and the acoustic pressure needs to be found in the second medium. In order to make the problem simple, assume the interface of the media is a flat plane as

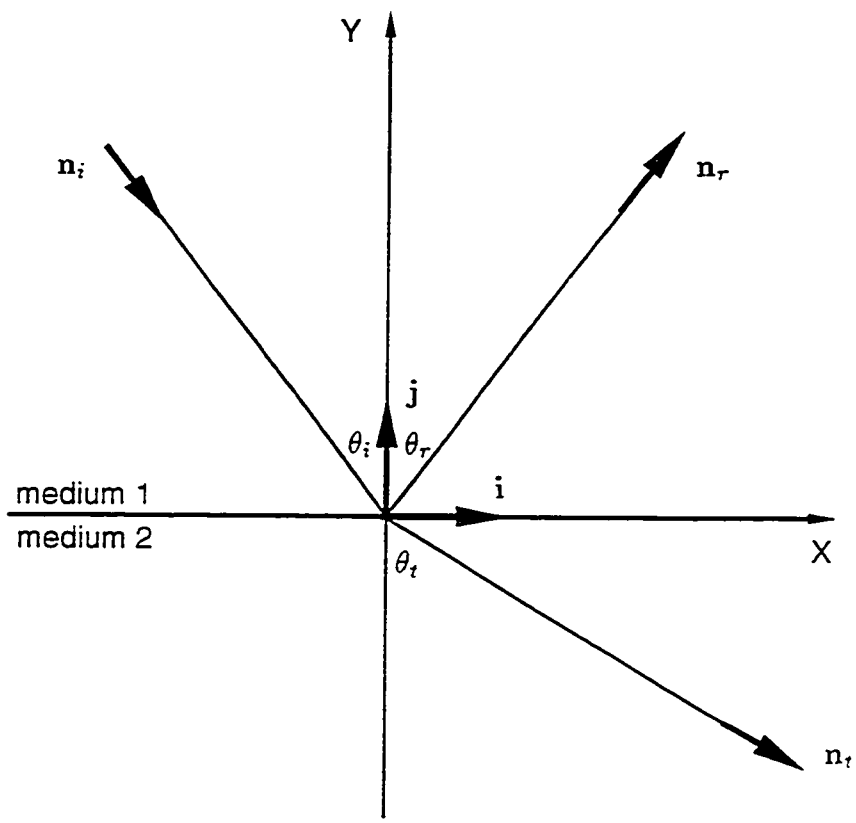

Figure 3. Acoustic wave incident on the interface of two media.

shown in Figure 4. The acoustic pressure in medium 1, just when the ray reaches the interface, is that of the direct wave alone, say $p_1(\theta_1)$, multiplied by the pressure transmission coefficient $T_1(\theta_1)$ (see Appendix A for detailed calculations), where

$$p_1(\theta_1) = \frac{f(t - r_1/c_1)}{r_1} \tag{5}$$

and

$$T_1(\theta_1) = \frac{2c_2\rho_2/\cos(\theta_2)}{c_2\rho_2/cos(\theta_2) + c_1\rho_1/\cos(\theta_1)}. \tag{6}$$

$f(t)$ is a function characteristic of the source. Thereafter, the ray moves with speed c_2 in direction θ_2 in medium 2 at depth H_2. The acoustic pressure at the point of interest can now be taken as the pressure at the interface with a new phase term, $t - r_1/c_1 - r_2/c_2$, times the transmission coefficient $T_1(\theta_1)$ and the amplitude diminution factor $A(\theta_1)$. The factor $A(\theta_1)$ is used to account for additional ray-tube spreading in the propagation from the interface to depth H_2. To determine $A(\theta_1)$ (see Appendix B for detailed calculations), consider two rays leaving the source at angles θ_1 and $\theta_1 + \delta\theta_1$, both rays having the same azimuth angle ϕ. They cross the interface at cylindrical distances W_1 and $W_1 + \delta W_1$ and subsequently propagate in the refracted directions θ_2 and $\theta_2 + \delta\theta_2$, where

$$W_1 = H_1 \tan(\theta_1) \qquad \text{and} \qquad \delta W_1 = H_1 \sec^2(\theta_1)\delta\theta_1. \tag{7}$$

The two rays cross the plane $z = H_1 + H_2$ at radial distances of W_2 and $W_2 + \delta W_2$, where by trigonometry theory,

$$W_2 = H_1 \tan(\theta_1) + H_2 \tan(\theta_2), \tag{8}$$

and

$$\begin{aligned} \delta W_2 &= H_1 \sec^2(\theta_1)\delta\theta_1 + H_2 \sec^2(\theta_2)\delta\theta_2 \\ &= [H_1 \sec^2(\theta_1) + H_2 c_2/c_1 \cos(\theta_1) \sec^3(\theta_2)]\delta\theta_1 \end{aligned} \tag{9}$$

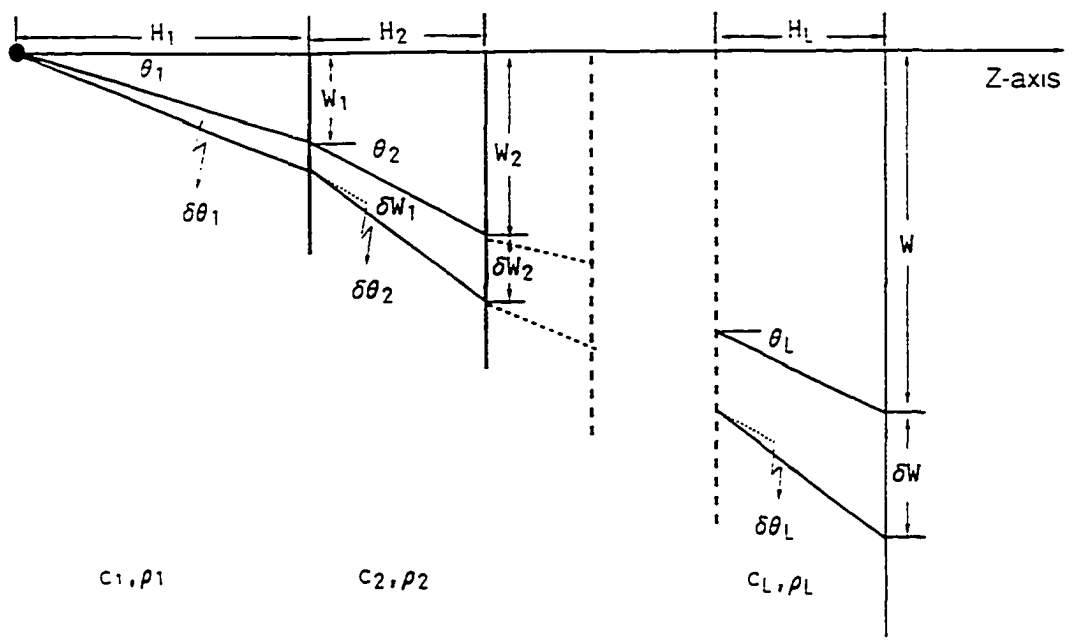

Figure 4. Diagram of the point source in a layered medium with regard to a Cartesian coordinate system.

The relation between $\delta\theta_1$ and $\delta\theta_2$ is given by the derivative of Snell's law.

$$c_2 \cos(\theta_1)\delta\theta_1 = c_1 \cos(\theta_2)\delta\theta_2 \tag{10}$$

The ray-tube area just before the ray crosses the interface is $(W_1\delta\phi)[\delta W_1 \cos(\theta_1)]$. Just after it crosses the interface the ray-tube area is $(W_1\delta\phi)[\delta W_1 \cos(\theta_2)]$. When it reaches depth $H_1 + H_2$, the ray-tube area is $(W_2\delta\phi)[\delta W_2 \cos(\theta_2)]$. Thus the ray tube area increases by a factor of $(W_2\delta W_2)/(W_1\delta W_1)$, in traversing just below the interface to the depth $H_1 + H_2$. Correspondingly, the pressure amplitude must be decreased by a factor of

$$A(\theta_1) = (W_1\delta W_1)^{1/2}/(W_2\delta W_2)^{1/2}. \tag{11}$$

In this manner, one obtains the acoustic pressure in medium 2 as

$$p_2(\theta_1) = A(\theta_1)T_1(\theta_1)\frac{f(t - r_1/c_1 - r_2/c_2)}{r_1}. \tag{12}$$

The above idea applied to an $L(> 2)$ layered medium, with $L-1$ flat plane parallel interfaces, allows the pressure in layer L to be written as:

$$p_L(\theta_1) = A(\theta_1)\prod_{j=1}^{L-1} T_j(\theta_j)r_1^{-1} f[t - \sum_{j=1}^{L}(r_j/c_j)], \tag{13}$$

where T_j is the acoustic pressure transmission coefficient in interface j, $r_j = H_j/\cos(\theta_j)$ is the ray path, c_j is the velocity of sound in medium j, and $A(\theta_1) = (W_1\delta W_1)^{1/2}/(W\delta W)^{1/2}$. Notice that equation (13) does not include the effect of attenuation. The angles θ_j can be found in terms of W and H_j from Snell's law. In general, this requires a numerical solution to solve a nonlinear system of equations. The equations are given by

$$\begin{cases} c_j \sin(\theta_{j+1}) = c_{j+1} \sin(\theta_j), \quad j = 1, 2, \cdots, L-1 \\ W = \sum_{j=1}^{L} H_j \tan(\theta_j) \end{cases} \tag{14}$$

for the L layered medium. The Newton-Raphson method (see Appendix C) is used to solve equation (14) (Press *et al.*, 1989). Equation (14) is a set of L equations with L unknowns. The angles are uniquely determined by c_j, H_j and W (see Appendix D for detailed calculations).

In order to apply the above idea to the ultrasound transducer, the surface of the transducer was divided into small elements so that each element could be treated as a point source. The integral in equation (1) has been evaluated by using Huygen's principle and summing the contributions from each element (Zemanek 1971). For each small element, using equations (1), (5) and (13), one can find the acoustic pressure in medium 1 and in medium L as

$$\Delta p_1(\theta_1^{mn}) = ik_1 c_1 \rho_1 v_s \frac{e^{-ik_1 r_1}}{r_1} e^{-\alpha_1 r_1} \Delta S^{mn} \tag{15}$$

$$\Delta p_L(\theta_1^{mn}) = \Delta p_1(\theta_1^{mn}) A(\theta_1^{mn}) \prod_{j=1}^{L-1} T_j(\theta_j^{mn}) \exp\left[-i\sum_{j=2}^{L} k_j r_j\right] \exp\left[-\sum_{j=2}^{L} \alpha_j r_j\right], \tag{16}$$

where ΔS^{mn} is the area of the small source element, θ_j^{mn} is the incident angle of the ray, k_j is the wave number and α_j is the linear amplitude attenuation coefficient in medium j. Notice that the effect of attenuation in each medium j was approximated by $e^{-\alpha_j r_j}$. The two mid-point rule was used to evaluate equation (1), i.e., sum all of the small elements over the area of the transducer. Now, the pressure in medium L for a whole transducer is given by

$$P_L = \sum_{m=1}^{M} \sum_{n=1}^{N} \Delta p_L(\theta_1^{mn}), \tag{17}$$

where $M \times N$ are the number of elements. At power levels in the linear ultrasound propagation range, the absorbed power is given by

$$Q = \mu_{abs} \frac{|P_L|^2}{Z_L}, \tag{18}$$

where μ_{abs} is the absorption coefficient and Z_L is the acoustic impedance of medium L. This numerical model to calculate the acoustic field for a layered medium with flat interfaces is used in this study.

2.3 Irregular interface model

The complex velocity potential from finitely sized exciting sources in a uniform medium can be calculated by the Rayleigh-Sommerfeld diffraction integral. The particle velocity along the radial direction can be obtained from the derivative of the velocity potential. In layered medium with irregular interfaces, the interface can be considered as a "Transducer" with normal particle velocities which was calculated according to Huygen's principle, i.e., the secondary wavefront was used to evaluate the velocities.

Consider a two layered medium, separated by a single surface, with velocities of sound c_i and densities ρ_i, $i = 1, 2$ (Figure 5). The complex acoustic velocity potential for a finitely sized exciting source, at the field of interest, point P_{f1} in medium 1, is given by (O'Neil, 1949)

$$\psi_1(r_1) = \frac{1}{2\pi} \iint_{S_1} v_{1_n} \frac{e^{-ik_{c1} r_1}}{r_1} ds_1. \tag{19}$$

Here the integration is over the whole radiating surface S_1, v_{1_n} is the normal excitation velocity on the radiator, $k_{c1} = k_1 - i\alpha_1$ is the complex wave number, $k_1 = \omega/c_1$ is the wave number, ω is the angular frequency, c_1 is the speed of sound, α_1 is the amplitude attenuation coefficient, and r_1 is the distance from the field point to the element area ds_1 of the radiator. The integral can be evaluated by using Huygen's principle and summing the contribution from incremental areas representing the radiating surface. The particle velocity along the radial direction r_1 at P_{f1} in medium 1 can be calculated by (Ristic, 1983)

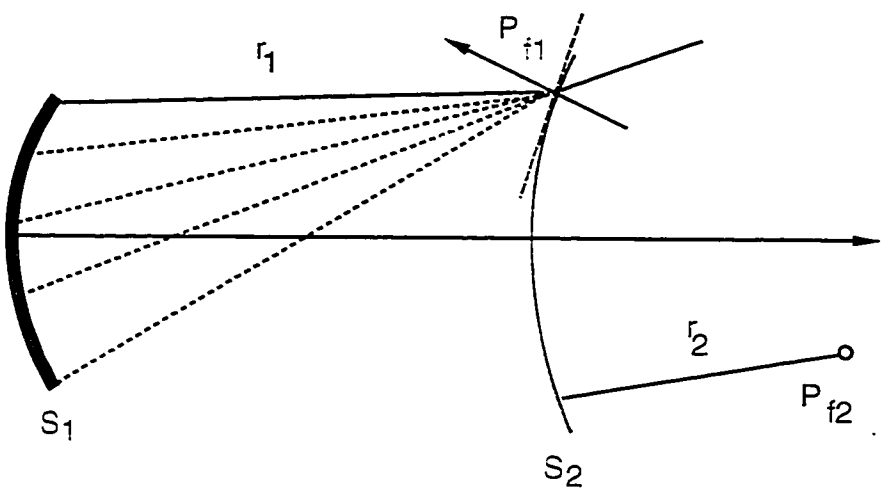

Figure 5. Two layered medium separated by an irregular interface.

$$v_2^- = -\partial\psi_1(r_1)/\partial r_1$$
$$= \frac{1}{2\pi}\iint_{S_1} v_{1_n}\frac{e^{-ik_{c1}r_1}}{r_1}\left(\frac{1}{r_1}+ik_{c1}\right)ds_1. \tag{20}$$

For each point on the interface S_2, the particle velocity in the radial direction, r_1, before reaching the surface, can be obtained from equation (20). The magnitude of v_2^- after crossing the surface will be reduced by the particle velocity transmission coefficient T_v. That is, the particle velocity on S_2 in medium 2 is equal to $v_2^- \times T_v = v_2^+$. Using Snell's law and the plane wave approximation, the particle velocity transmission coefficient is given by (see Appendix A for detailed calculations)

$$T_v = \frac{2\rho_1 c_1 \cos(\theta_1)}{\rho_2 c_2 \cos(\theta_1) + \rho_1 c_1 \cos(\theta_2)}, \tag{21}$$

where the θ_i, $i = 1,2$ is the incident and transmission angles, respectively, referenced to the normal of the surface S_2. The normal particle velocity, v_{2n}, on S_2 just across the surface due to the exciting source S_1 is

$$v_{2_n} = v_2^+ \cos(\theta_2) = v_2^- T_v(\theta_1)\cos(\theta_2). \tag{22}$$

Using equation (20) and dividing S_1 into $M \times N$ small area elements ΔS_1^{mn}, which are treated as point sources, equation (22) becomes

$$v_{2_n} = \frac{1}{2\pi}\sum_{m=1}^{M}\sum_{n=1}^{N} v_{1_n}\frac{e^{-ik_{c1}r_1}}{r_1}\left(\frac{1}{r_1}+ik_{c1}\right)\Delta S_1^{mn} T_v(\theta_1^{mn})\cos(\theta_2^{mn}), \tag{23}$$

where θ_1^{mn} and θ_2^{mn} are incidence and transmission angles for each ΔS_1^{mn}. The complex velocity potential in medium 2, at the point of interest P_{f2}, can then be calculated by using equation (19)

$$\psi_2(r_2) = \frac{1}{2\pi}\iint_{S_2} v_{2_n}\frac{e^{-ik_{c2}r_2}}{r_2}ds_2, \tag{24}$$

where k_{c2} is defined in the same way as k_{c1}, and r_2 is the distance from the element area ds_2 to the field point P_{f2}. Notice that the surface S_2 can be considered as a new radiator. The integration in equation (24) is calculated as in equation (23). The above idea can be expanded to multiple layers. The acoustic pressure in medium 2 is then calculated by

$$P_2 = \rho_2 \partial\psi_2/\partial t = i\omega\rho_2\psi_2 = ik_2 Z_2 \psi_2, \tag{25}$$

where $Z_2 = \rho_2 c_2$ is the acoustic impedance of medium 2. Finally, the absorbed power density is calculated by

$$Q = \mu_{abs}\frac{|P_2|^2}{Z_2}. \tag{26}$$

For simulation purposes in hyperthermia, when a focused transducer is used, the surface S_2 can be considered a finite size and divided into small area elements. In this way the single ultrasound wave reflection and refraction at the irregular interfaces can be handled. All the simulation results were calculated by using the CONVEX C240 mini-supercomputer at the University of Arizona Computer Center.

CHAPTER 3

3. EXPERIMENT

3.1 Measurements

3.1.1 Acoustic power measurement

A power transmission test was performed on polyethylene sheets of different thickness. These sheets were large enough in their lateral dimension so that all the power passed through it. Measurements were done twice, with and without the plastic. The equipment used to produce these results, consisted of the transducer, an absorbing target, and an electronic balance (Metter, Model AE 160). The plastic sheet was placed between the transducer and the absorbing target, which were both in the tank filled with degassed water. The average acoustic power was computed at each different electrical input power level (see (Stewart 1982) for a review of the acoustic power measurements). The natural logarithm of the transmitted power was then plotted as a function of the thickness of the plastic with the attenuation coefficient calculated from the slope (m) of the straight line, $\alpha = -m/2$ (Fry and Dunn 1962).

3.1.2 Ultrasound field measurement

The relative pressure amplitude squared distributions in a water bath were obtained by scanning an ultrasound detector along a raster pattern under computer control. A thermocouple embedded in a small plastic bead was used to detect the field during continuous wave ultrasound pulses (pulse length 60 ms)

(Martin and Law 1983). The thermocouple probe was moved by stepper motors, typically with 0.5 mm steps across the beam and 2 mm steps in the axial direction. In order to reduce the electrical noise, five pulses were emitted at each thermocouple location to obtain an average value at that position. The experiment was performed twice: first, in water only; and second, with polyethylene in front of the transducer to simulate a layered medium. Air-backed transducers (Table 1) were driven using an RF pulse/function generator (Wavetek model 271) and an RF power amplifier (ENI model 240L). The overall process was supported by a Hewlett Packard laboratory computer system (9000 computer, 3456A digital voltmeter, 3497A acquisition unit). All the transducers were electrically matched to the amplifier's output impedance by using a passive matching network. The voltage applied to the transducer was kept high enough to obtain a good signal and low enough to avoid cavitation or nonlinear effects.

3.1.3 Speed of sound measurement

The speed of sound in polyethylene was measured in a water tank by passing sound through blocks of different thicknesses of polyethylene. The equipment used in the measurements were: a flat transducer (air-backed), RF pulse/function generator (Wavetek model 271), RF power amplifier (ENI model 240L), hydrophone and digital storage oscilloscope (Tektronix 336). First, the time of flight of a sound pulse from the transducer to the hydrophone was measured. Second, a polyethylene block of known thickness was inserted between the transducer and hydrophone and the time of flight of the second pulse was measured. The speed of sound in the polyethylene was determined using

$$c_p = \frac{L}{L/c_w + \Delta t}$$

	Frequency (MHz)	Diameter (cm)	Radius of Curvature (cm)
Transducer 1	0.5	7.0	35.0
Transducer 2	0.558	10.0	10.0
Transducer 3	1.0	7.0	25.0
Transducer 4	0.5,1.0,2.0	10.0	10.0
Transducer 5	1.75	10.0	20.0

Table 1. Ultrasound transducers used in the experiments and simulations.

Material	Thickness (cm)	Density (kg/m^3)	Speed of Sound (m/s)	Amplitude Attenuation Coefficient $(Np/m/MHz)$
Ultra-high	4.88			
Molecular	2.00			
Weight	1.27	938.0[a]	2210.0[b]	21[b]
Polyethylene	0.97			

Sources: [a]Modern plastics encyclopedia 1990. [b] Measured.

Table 2. Plastic sheets used in the experiments and simulations.

where L is the thickness of the polyethylene, c_w is the speed of sound in water, Δt is the second time of flight minus the first. Notice that the Δt is a negative number. The measured speed of sound of polyethylene was 2210 (m/s) with a standard deviation of 20 (m/s).

3.2 Simulation models

3.2.1 Flat plane interfaces

In order to verify the layered numerical model and investigate the effect of soft tissue interfaces on the ultrasound wave propagation, two models were used in this thesis.

Water-polyethylene-water model : This three layered medium has flat plane interfaces with a water temperature of $22°C$ and the thickness of the polyethylene being 4.88 and 1.27 cm (Figure 6A). The properties of polyethylene are given in Table 2. Transducer 1 and 2 were used in the experiments and numerical simulations with different incidence angles.

Water-skin-fat-muscle model : This four layered medium has flat plane interfaces with various fat layer thicknesses, water temperatures and tissue temperatures (Figure 6b). The properties of the tissue are given in Table 3-5. Transducer 3 and 4 were used in the numerical simulations with different incidence angles. The speed of sound as a function of temperature is varied as shown in Table 6. The density of water is 998 (kg/m^3).

3.2.2 Curved interfaces

A half polyethylene tube was used to simulate the curved interfaces and verify the numerical model similarly as in Section 3.2.1.

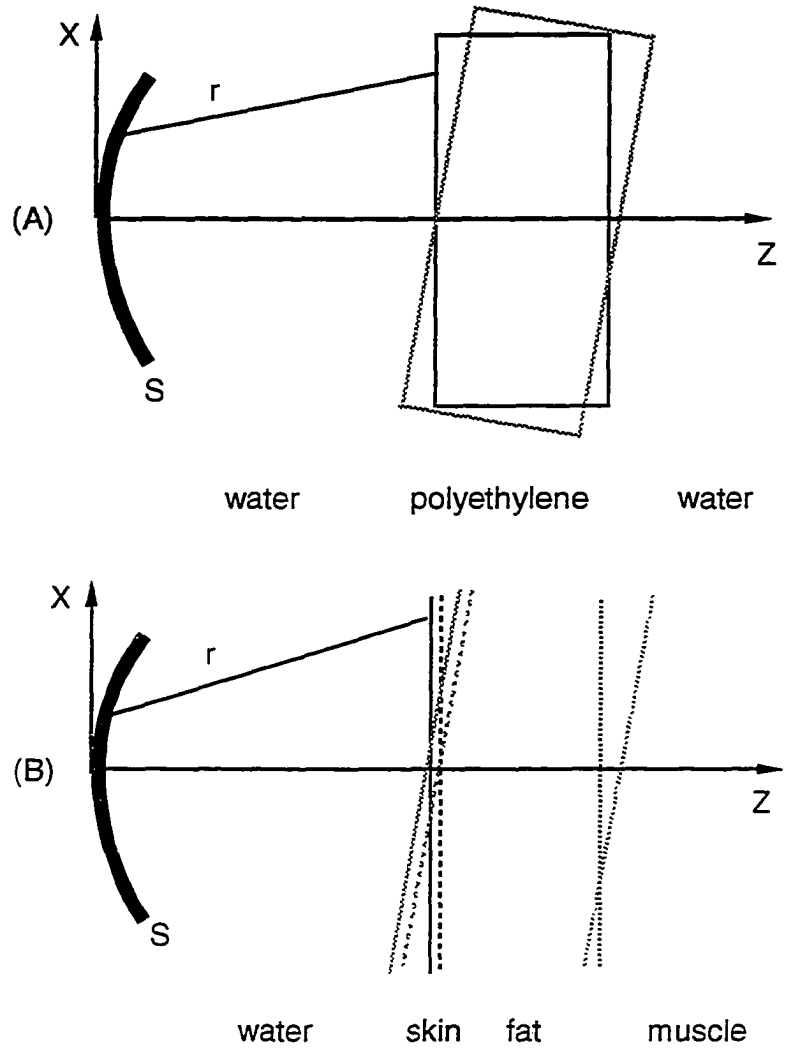

Figure 6. Diagram of parallel flat plane interface models used in the experiments and simulations. The Z-axis is defined in the axial direction, the X-axis is defined in the radial direction, the Y-axis is pointed out of the paper and parallel to the interface of the medium. Notice that the ultrasound field is symmetry about the X-Z plane and the transducer can be tilted. (A) water-polyethylene-water three layers, (B) water-skin-fat-muscle four layers.

Tissues	Velocity (m/s)	Attenuation (Np/m)	Density (kg/m^3)	Absorption (Np/m)
Bone	$1500-3700$	$150-350$	$1380-1810$	–
Brain	$1516-1575$	$4-29$	1030	$1.2^d-6.4^e$
Fat	$1400-1490$	$5-9$	921	–
Liver	$1540-1640$	$3.2-18$	1060	$2.3-3.2$
Muscle	$1508-1630$	$4.4-15^b$	$1070-1270$	$2-11$
Skin	1498^a	$14-66^c$	1200	–

Temperature: $^a23°C$, $^b40°C$, ^{c} not reported.

Brain: ^{d}grey matter, ^{e}white matter.

Source: Goss *et al.* 1978, 1979, 1980; Chivers and Parry 1978; Lyons and Parker 1988; Wells 1977.

Table 3. Acoustic properties of mammalian tissues at a temperature of $37°C$ and a frequency of 1 MHz.

Tissues	Thickness (cm)	Velocity (m/s)	Attenuation ($Np/m/MHz$)	Density (kg/m^3)
Bone	*various*	2600	150	1595
Brain	*various*	1545	4	1030
Fat	$0.0 - 3.0$	1445	7	921
Muscle	*various*	1569	9	1138
Skin	0.17	1498	14	1200

Table 4. The specific values of tissue properties used in the simulations.

Tissues	Temperature ($°C$)	Velocity (m/s)	Attenuation (Np/m)
Bovine liver	37	1597	17 (*approx.*)
	43	1595 (*approx.*)	17 (*approx.*)
Bovine fat	37	1430	12 (*approx.*)
	43	1400 (*approx.*)	12 (*approx.*)

Source: Bamber and Hill (1979).

Table 5. Tissue properties for variation of temperature at 1 MHz.

Temperature ($°C$)	Speed of sound[α] (m/s)
5.0	1426.1
15.0	1465.9
20.0	1482.3
25.0	1496.6
26.3	1500.0
35.0	1519.8
37.0	1523.6
43.0	1533.5
45.0	1536.4

[α]All data rounded to the nearest one-tenth.

Source: Del Grosso and Mader (1972).

Table 6. Sound speed in pure water.

Water-polyethylene-water : This three layered medium has two curved interfaces with the corresponding radius of curvatures of 5 cm and 3 cm (Figure 7A). The water temperature was $22°C$.

In order to gain an understanding for the ultrasound hyperthermia treatments of tumors, five anatomical geometries were studied: (1) a brain model, (2) a neck model, (3) a body model, (4) a buttocks model, and (5) a bone model.

Brain model : The brain model was a sphere containing two layers: skin and brain. The radius of curvature of the sphere was 9 cm and the skin thickness was 1.7 mm.

Neck model : The neck model was a cylinder containing two layers: fat and muscle. The radius of curvature of the cylinder was 7 cm and the fat layer thickness was 1 cm.

Body model : The body model was the same as the neck model except that the radius of curvature was 15 cm and the fat layer thickness was 2 cm.

Buttocks model : The buttocks model had two layers: fat and muscle, with spherical interfaces. The radius of curvature was 10 cm. The fat layer thickness was 3 cm.

Focused transducers were used during the treatment simulations. First the transducer axis was aimed through the center of the geometry, then the transducer was moved toward the edge of the geometry while keeping the focal distances the same (Figure 7B).

Bone model : The bone model was one layer (muscle) with the bone positioned on the transducer axis and behind the focus. The bone was a cylinder with a radius of curvature of 1 cm (Figure 7C).

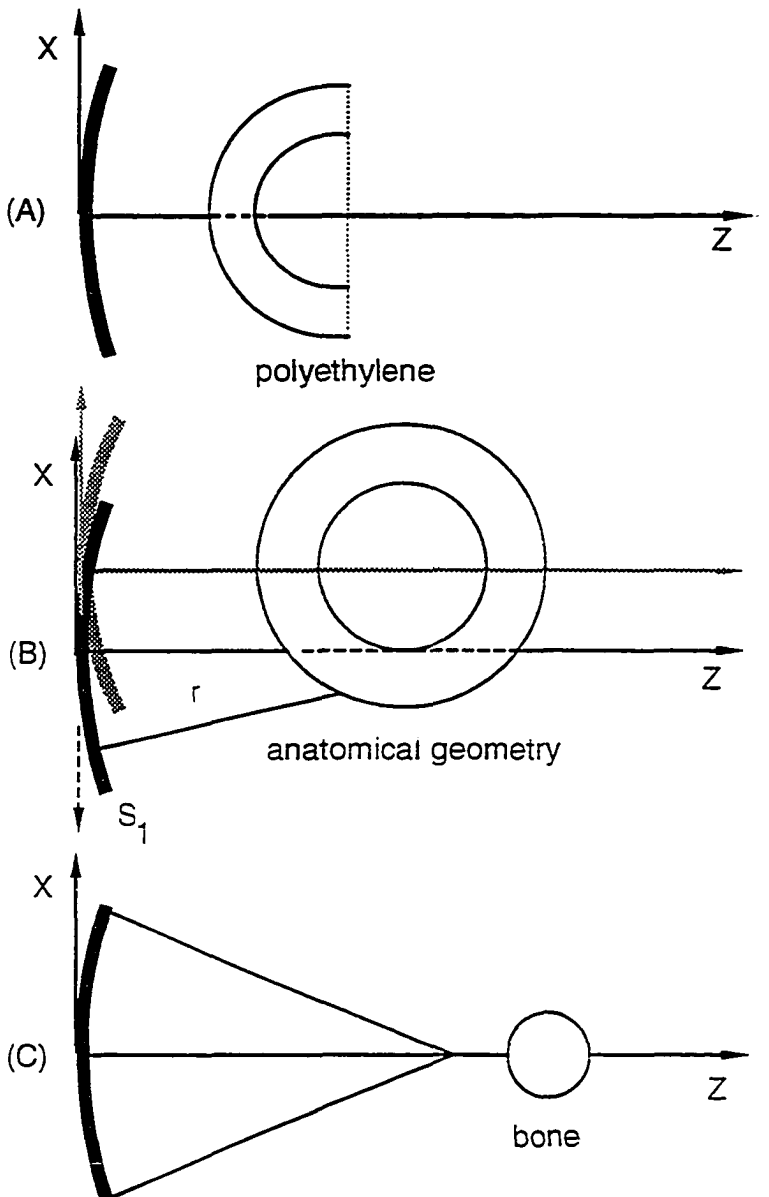

Figure 7. Diagram of curved interface models used in the experiments and simulations. The Z-axis is defined in the axial direction, the X-axis is defined in the radial direction, and the Y-axis is pointed out of the paper. (A) water-polyethylene-water three layers, (B) anatomical geometries, except bone model, (C) bone model.

CHAPTER 4

4. RESULTS

4.1 Comparison between the theory and the experiment

4.1.1 Layered model

The square of the acoustic pressure amplitude distribution across the focus of two transducers has been measured in water with a polyethylene plate between the transducer and the focus to test the ability of the model to predict the effect of layered medium. Examples of the experimental and theoretical results are displayed in Figures 8,9 and 10. In Figure 8 the normalized ultrasound pressure amplitude squared distributions across the acoustical focus of transducer 1 are presented with the polyethylene plate (thickness is 4.88 cm) at different angles with respect to the surface of the transducer. Both theory and experiments were normalized to their peak value in water without the plate. Similar graphs for transducer 2 are presented in Figure 9 with a 1.27 cm thick plate. For this transducer the measurements are taken with two angles only, due to the physical constraints of the measurement arrangement. In Figure 10, the ultrasound field distributions measured and calculated in the axial plane are given for the case presented in Figure 9B. The theoretical ultrasound field appeared to be slightly more narrow and the focus about 1 mm deeper than measured in the experiments. This trend is typical, that is the experimental focus is closer to the transducer than the theory predicted. This agrees with earlier waterbath measurements and

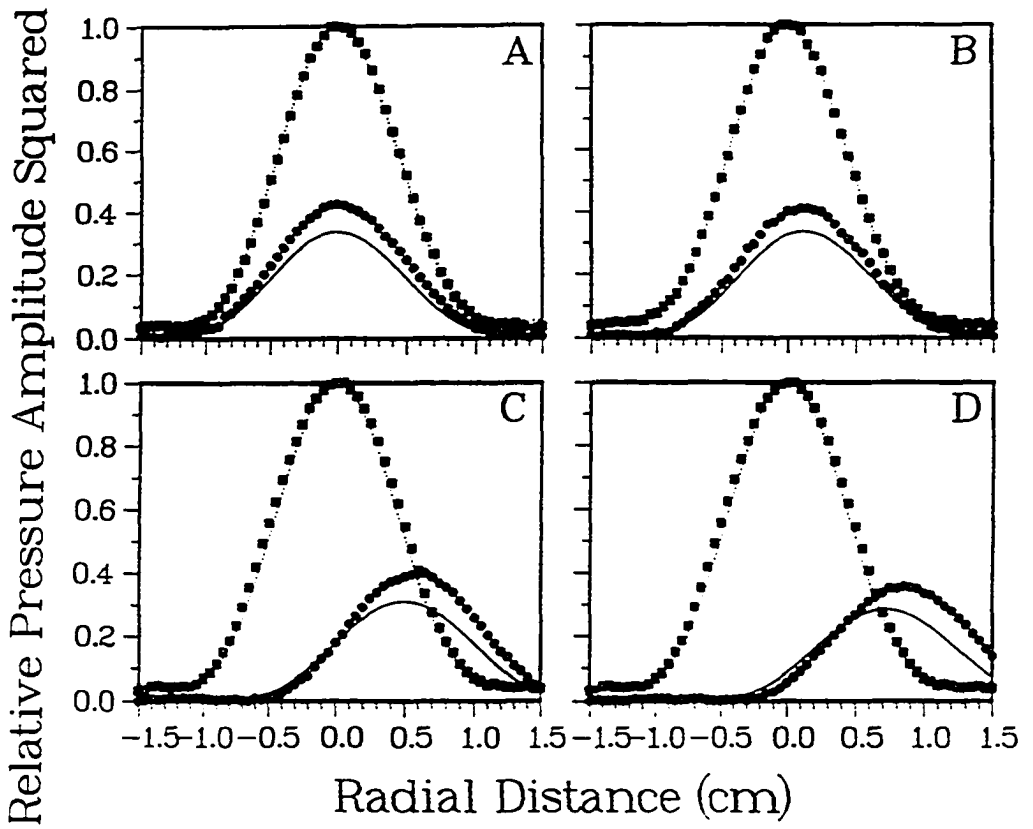

Figure 8. The theoretical and experimental normalized square of pressure amplitude response as a function of radial distance at the acoustic focus. The 35 cm radius of curvature and 7 cm diameter transducer has been used with a frequency of 0.5 MHz. The points correspond to the experiments and the smooth lines to the theory. The data is normalized to the peak value in water (both theoretical and experimental to its own value) and thus, the curves with a peak value of 1 are for the water only case and the other curves are for the water-polyethylene-water model. The thickness of the polyethylene is 4.88 cm. The angle between the transducer face and the interface of the media is : (A) 0°, (B) 4°, (C) 15°, (D) 20°.

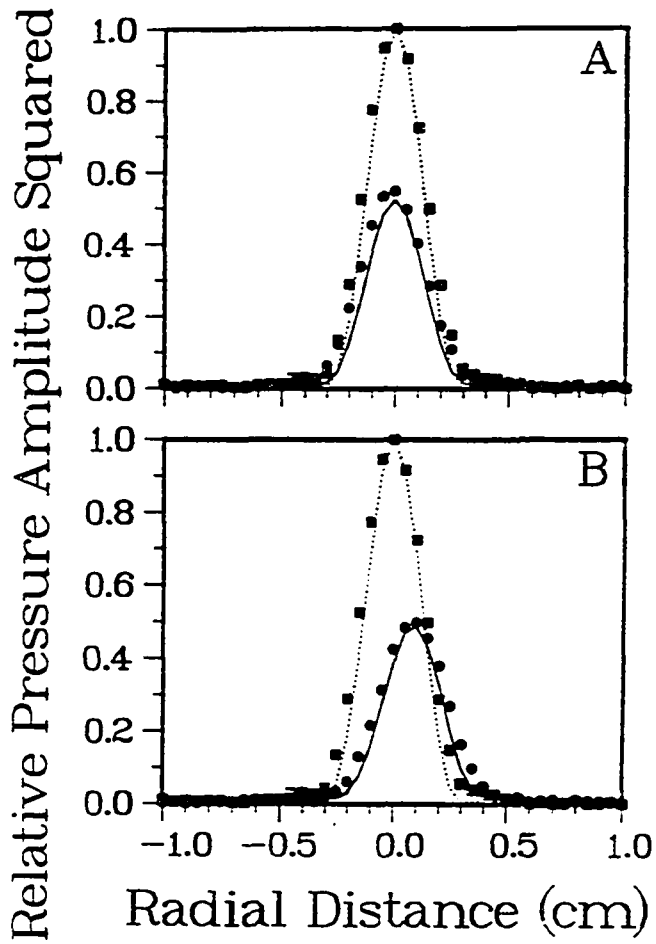

Figure 9. The theoretical and experimental normalized square of pressure amplitude response as a function of radial distance at the acoustic focus. The 10 cm radius of curvature and 10 cm diameter transducer has been used with a frequency of 0.558 MHz. The points correspond to the experiments and the smooth lines to the theory. Curves with a peak value of 1 are for the water (data normalized to the peak value in water) only case and the other curves are for the water-polyethylene-water model. The thickness of the polyethylene is 1.27 cm. The angle between the transducer face and the interface of the media is: (A) 0°, (B) 8.7°.

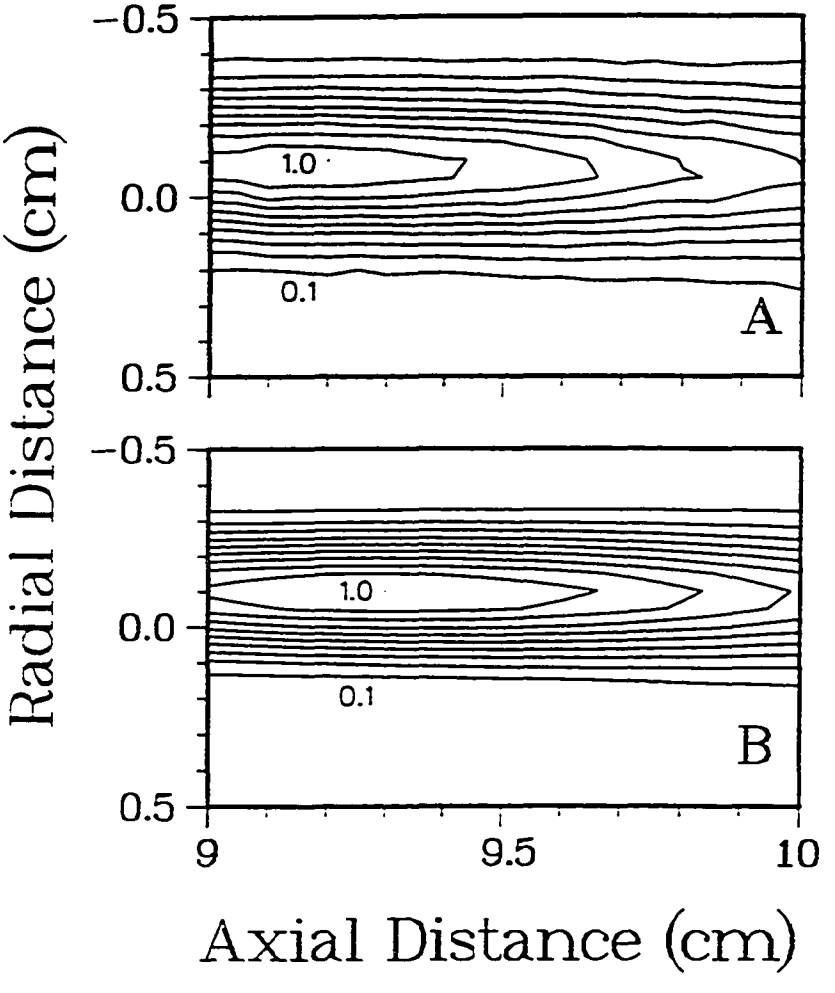

Figure 10. The contour plot of the relative pressure amplitude squared distribution for the water-polyethylene-water case: (A) experiment, (B) simulation. The conditions are the same as in Fig. 9 (B).

ultrasound field calculations (Moros and Hynynen 1991). Overall these results indicate that the theoretical relative ultrasound field distributions across the focus agree well with the measured distributions in water. The effect of the polyethylene plate is also well predicted at various angles. Thus, it appears that this program can be used to model the effect of different soft tissue layers on the relative ultrasound field distributions.

4.1.2 Irregular model

The acoustic pressure amplitude squared distribution across a focus of the transducer has been measured in water with a half polyethylene tube (thickness is 2 cm) between the transducer and the focus to verify the numerical model to predict the effect of curved interfaces. An example of the experimental and theoretical results are shown in Figures 11 and 12. Both theoretical and experimental values were normalized to their peak value in water without the polyethylene. In Figure 11 transducer 1 was used and the distance from the center of the polyethylene-tube to the acoustic focus was 1.1 cm. When the transducer axis moved from the center of the polyethylene-tube to its edge, the ultrasound field distribution distorted and shifted 1.5 mm in the lateral direction. In Figure 12 transducer 2 was used and the distance from the center of the polyethylene-tube to the acoustic focus was 1.4 cm. When the transducer axis moved from the center of the polyethylene-tube to its edge, the ultrasound field shifted 2 mm. For this strongly focused transducer, when the transducer axis was 2 cm away from the center, the magnitude reduced 60% from the case in which the transducer axis was aimed through the center. The simulation and experimental results agreed very well. The effect of the curved surface on the ultrasound wave propagation is also well predicted.

4.2 Comparison with the simplified model

Since the simplified model developed by Swindell *et al.* (1982) has been extensively tested in water and in tissue (Moros and Hynynen 1991), it was used to compare with the new models. The simplified model is theoretically accurate in nonattenuating medium such as water and thus, all of the models should give identical ultrasound field distributions in water. The simulation results verified this, giving similar (within the numerical accuracy of the calculations) absolute pressure amplitude values for all of the models (Table 7).

However, the simplified model does not take the tissue interfaces into account and assumes uniform ultrasound velocity throughout the medium. In addition, the attenuation factor has some theoretical inaccuracy as shown in Section 2.1. To estimate how these factors influence the ultrasound fields, the simplified model was compared with a water-tissue two layered model with the interface parallel to the transducer (Figure 13). Three cases were simulated with the new model: First, the speed of sound and the acoustic impedance were kept constant to give an idea of the error associated with the attenuation approximation. Generally, the simplified model overpredicted the peak pressure amplitude squared value. The maximum error in the overprediction was about 7% with the f-number 1 transducer and decreased with reduced focussing. This error decreased to about 1% with an f-number 3.6 transducer. The percentage difference increased linearly with frequency up to 25% for an f-number 1 transducer at a frequency of 3 MHz.

Second, the speed of sound in tissue was reduced to 1400 m/s. This change moved the focus about 5 mm deeper (at a depth of 50 mm in tissue) and reduced the peak value by an additional 10%. This reduction was not f-number dependent. Third, the speed of sound in tissue was increased to 1600 m/s. This caused a

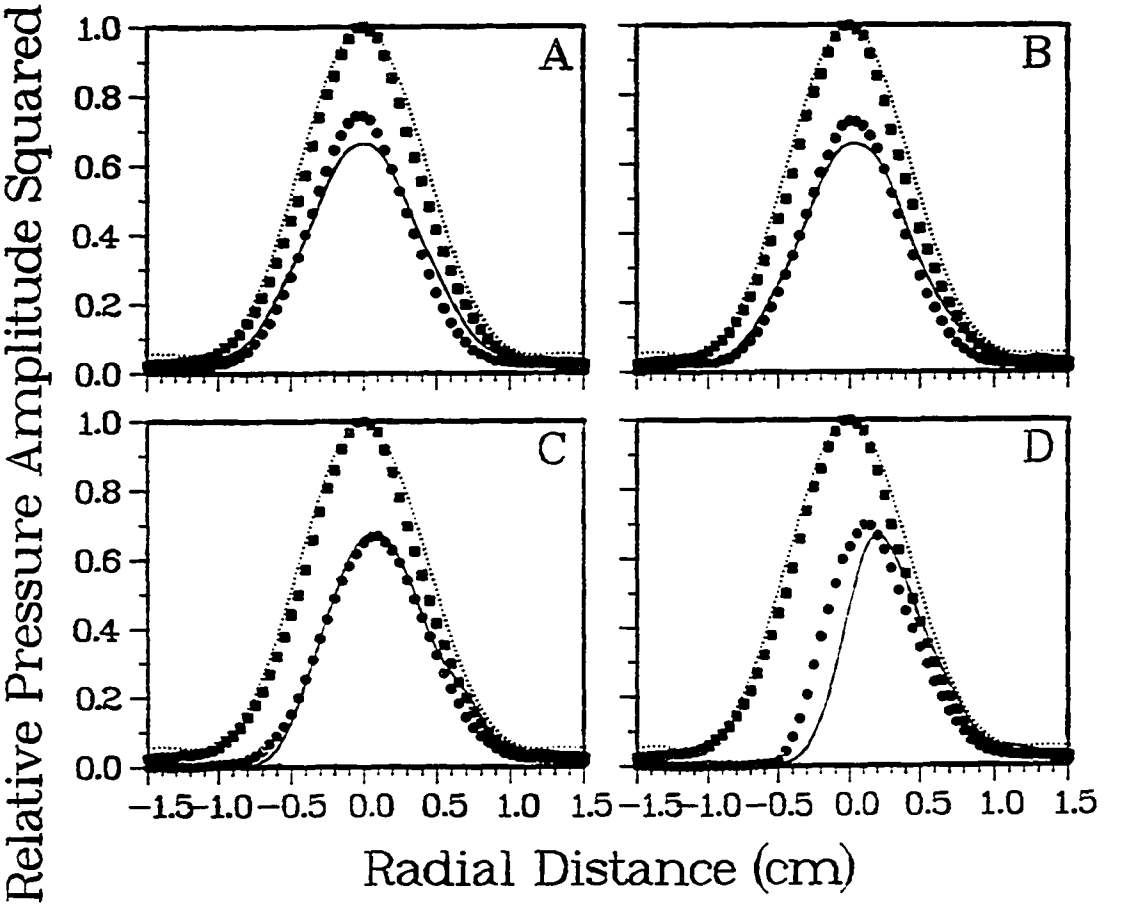

Figure 11. The theoretical and experimental normalized square of pressure amplitude response as a function of radial distance at the acoustic focus. The 35 cm radius of curvature and 7 cm diameter transducer has been used with a frequency of 0.5 MHz. The points correspond to the experiments and the smooth lines to the theory. Curves with a peak value of 1 are for the water (data normalized to the peak value in water) only case and the other curves are for the water-polyethylene-water model. The distance between the center of the polyethylene-tube and the transducer axis is : (A) 0.0 cm,(B) 0.5 cm, (C) 1.0 cm, and (D) 1.5 cm.

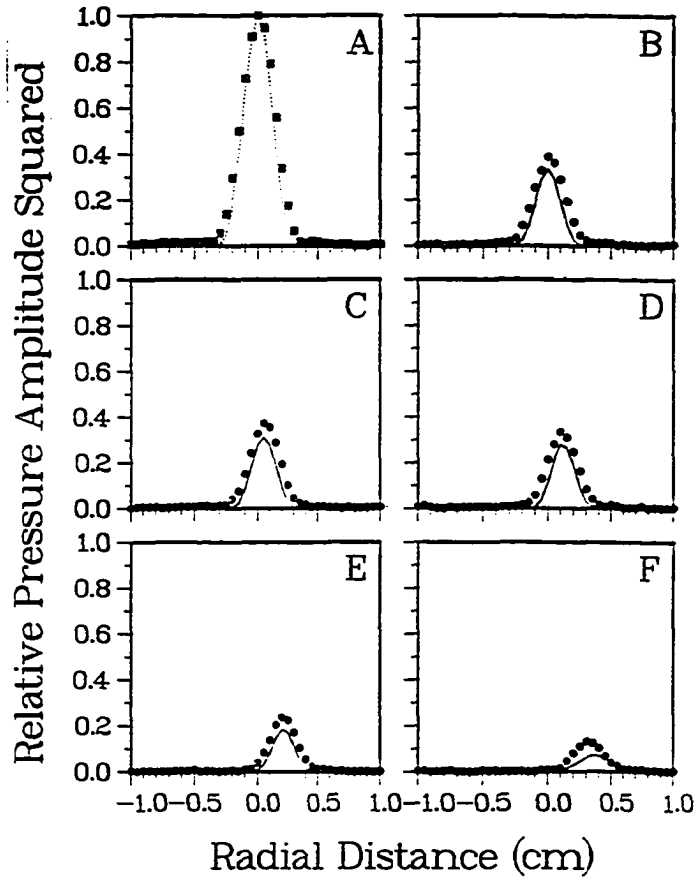

Figure 12. The theoretical and experimental normalized square of pressure amplitude response as a function of radial distance at the acoustic focus. The 10 cm radius of curvature and 10 cm diameter transducer has been used with a frequency of 0.558 MHz. The points correspond to the experiments and the smooth lines to the theory. Curves with a peak value of 1 are for the water (data normalized to the peak value in water) only case (A) and the other curves are for the water-polyethylene-water model. The distance between the center of the polyethylene-tube and the transducer axis is : (B) 0.0 cm,(C) 0.5 cm, (D) 1.0 cm, (E) 1.5 cm, and (F) 2.0 cm.

Frequency (MHz)	Diameter (cm)	Radius of Curvature (cm)		Simplified Model (Pressure	Layered Model Amplitude	Irregular Model Squared)
0.5	7.0	35.0		1.000000	0.9978949	1.025474
			CPU-Time(s)	4.7×10^{-4}	0.5366810	101.7891
0.558	10.0	10.0		1.000000	1.000005	1.001149
			CPU-Time(s)	3.7×10^{-4}	1.067264	208.6746
1.0	7.0	25.0		1.000000	0.9992149	1.004764
			CPU-Time(s)	4.3×10^{-4}	1.058572	208.5341
1.0	10.0	10.0		1.000000	1.001373	0.9990781
			CPU-Time(s)	3.8×10^{-4}	1.067795	210.1394
3.0	7.0	35.0		1.000000	1.001286	0.9999449
			CPU-Time(s)	3.5×10^{-4}	1.039538	427.2026

Note: The accuracy of CPU time is in microsecond.

Table 7. Comparison of three models in water. The relative square of pressure amplitude distribution at the acoustic focus was computed for each transducer with given frequency. The data are normalized by the simplified model's results.

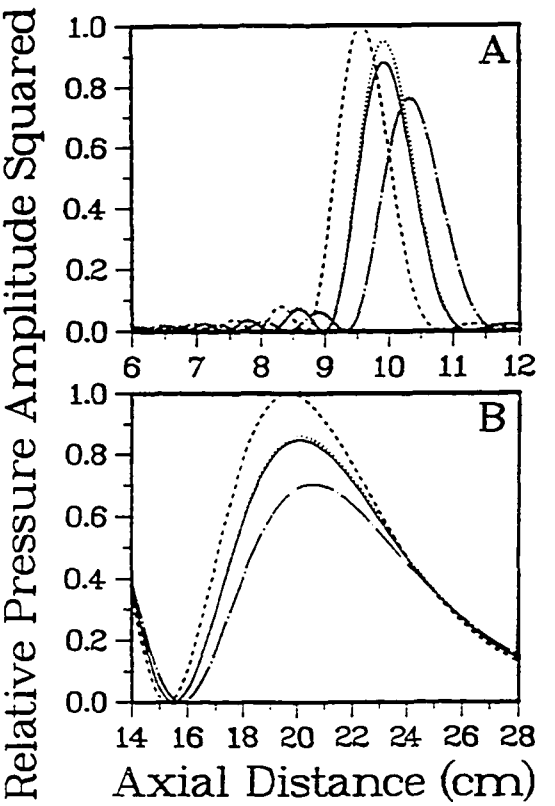

Figure 13. Square of relative pressure amplitude response as a function of the axial distance in water-tissue model calculated with three different methods. 1) Simplified model (dotted line), 2) 2-dimensional integration (solid line), 3) 2-dimensional integration with sound speed in water 1500 m/s and tissue 1600 m/s (dashed line), 4) same as method 3 but with the sound speed in tissue being 1400 m/s (chained line). The attenuation was 0.1 Np/cm/MHz. (A) The transducer had a 10 cm radius of curvature and a 10 cm diameter. The interface is 5.0 cm from the transducer. (B) The transducer had a 25 cm radius of curvature and a 7 cm diameter. The interface is 12 cm from the transducer. The frequency is 1 MHz for both cases.

similar change in the ultrasound field distribution except that now the peak pressure value was increased (from the 1500 m/s value) and its location was moved closer to the transducer.

4.3. Effects of multiple tissue layers and coupling water temperature

In order to simulate patient treatments, a water-skin-fat-muscle (WSFM) four layered model was used. With this model several parameters were varied to obtain guidelines for clinical ultrasound hyperthermia treatments. First, the effect of the thickness of the fat layer on the axial ultrasound field distribution was studied when the beam was normal to the surface of the tissue layer (Figure 14A). From the results it appears that an increase in the fat layer will shift the peak value of the ultrasound field further away from the transducer. For the f-number 1 transducer, the increase in focal depth was about 2.5 mm when the fat-layer was increased from 0 to 3 cm. The peak value increased slightly.

Second, the effect of the coupling waterbath temperature on the axial ultrasound field distribution was studied with three different frequency ultrasound fields (Figure 14 B-D). The increase in the water temperature moved the focus deeper and also reduced the absolute peak value of the field. The maximum difference in the focal location was 5 mm (focussed at a distance of 50 mm from the tissue surface) and the reduction in the peak value was about 20% when the temperature was increased from $5°C$ to $45°C$. The effect of the water temperature appeared to increase with increased frequency.

Third, the effect of variation in tissue temperature on the axial and radial ultrasound field distribution was studied with two different temperatures (Figure 15). The water temperature was fixed at $26.3°C$. When the tissue temperature

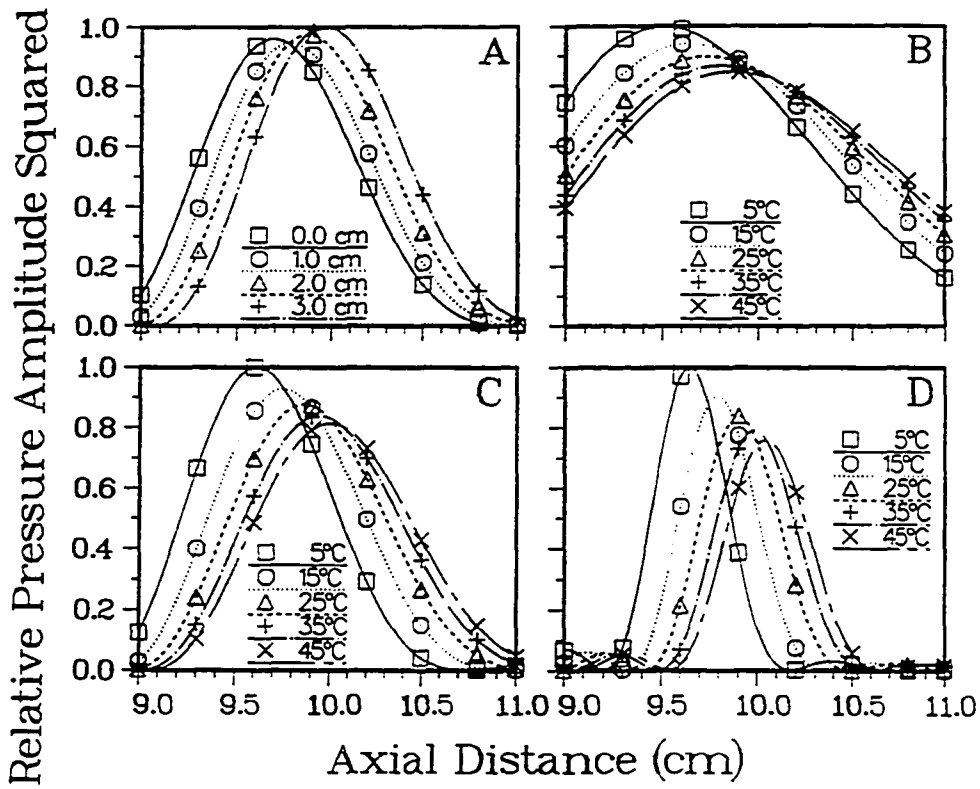

Figure 14. Relative pressure amplitude squared as a function of axial distance in the water-skin-fat-muscle (WSFM) layered model. The transducer was 10 cm in diameter and had a 10 cm radius of curvature. The distance from the transducer to the skin was 5 cm. (A) fat thickness changed from 0 to 3 cm. Frequency was 1 MHz. (B), (C), (D) fat thickness was 1 cm. Water temperature changed from 5 to 45 degrees. The frequency was: (B) 0.5 MHz; (C) 1 MHz; (D) 2 MHz. The angle of incidence was 0° in all cases. The properties of the tissue are given in Table 4.

changed from $37°C$ to $43°C$, the peak value was reduced by about 5%, and the focus was moved about 1 mm deeper.

Finally, the effect of the tilt angle between the tissue surface and the propagation direction of the wave was investigated as a function of the fat layer thickness and the coupling water temperature. Figure 16 shows the ultrasound field distributions along the axial plane for three different tilt angles for one transducer. The fat layer thickness was 10 mm and the coupling water temperature was $26.3°C$. In these graphs a radial distance of 0 indicates the location of the geometric central axis of the beam in uniform medium. These results clearly indicate that the layered medium has a significant effect on the ultrasound field distribution mainly shifting it off axis and distorting the radial symmetry of the beam especially at the larger angles. Figure 17 shows the effect of the tilt angle on the peak value of the field with two different fat layer thicknesses and coupling water temperatures. The peak value appears to increase slightly as a function of angle until it peaks at around 60° and then drops rapidly. The thickness of the fat layer and the coupling water temperature has only a slight effect on the curves. Similar graphs for the distance of the peak ultrasound field value from the central axis are given in Figure 18. The off-axial displacement is a strong function of the angle and can reach as much as 6 mm at angles about 60°. However, the magnitude of the displacement depends on the fat layer thickness and the coupling water temperature.

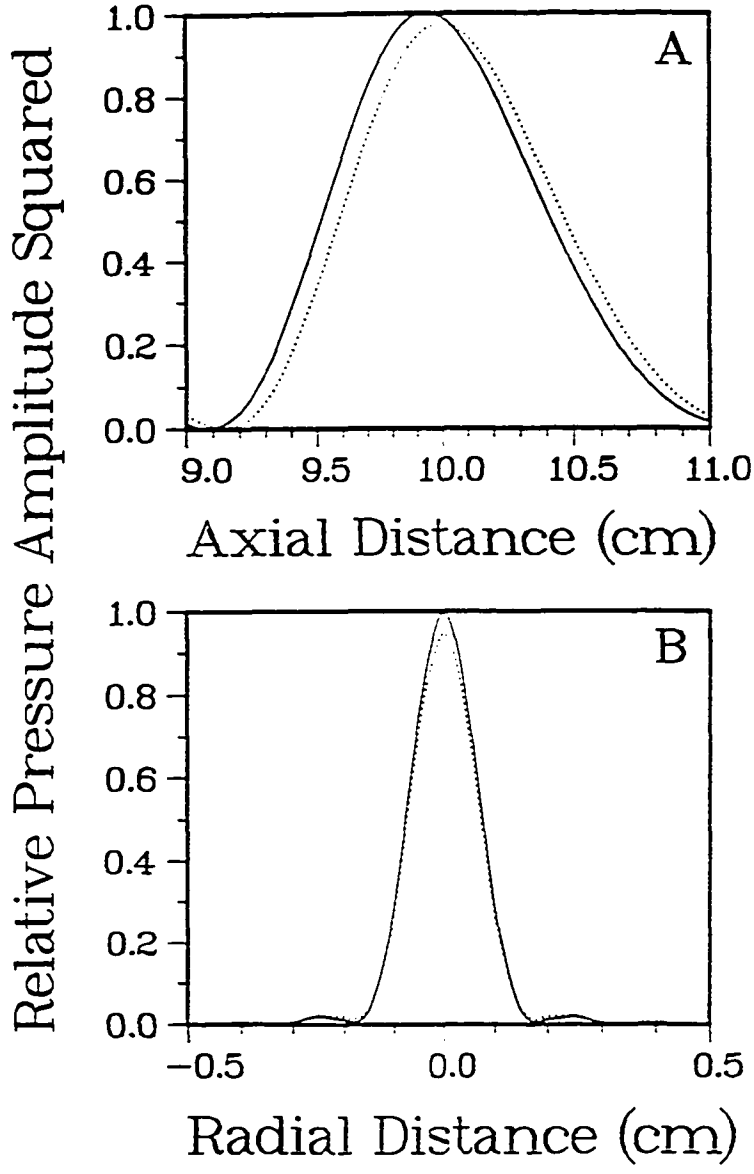

Figure 15. Relative pressure amplitude squared as a function of axial (A) and radial (B) distance in water-skin-fat-liver layered model. The transducer was 10 cm in diameter with a 10 cm radius of curvature. The distance from the transducer to the skin was 5 cm. The frequency was 1 MHz (—— 37°C, ····· 43°C).

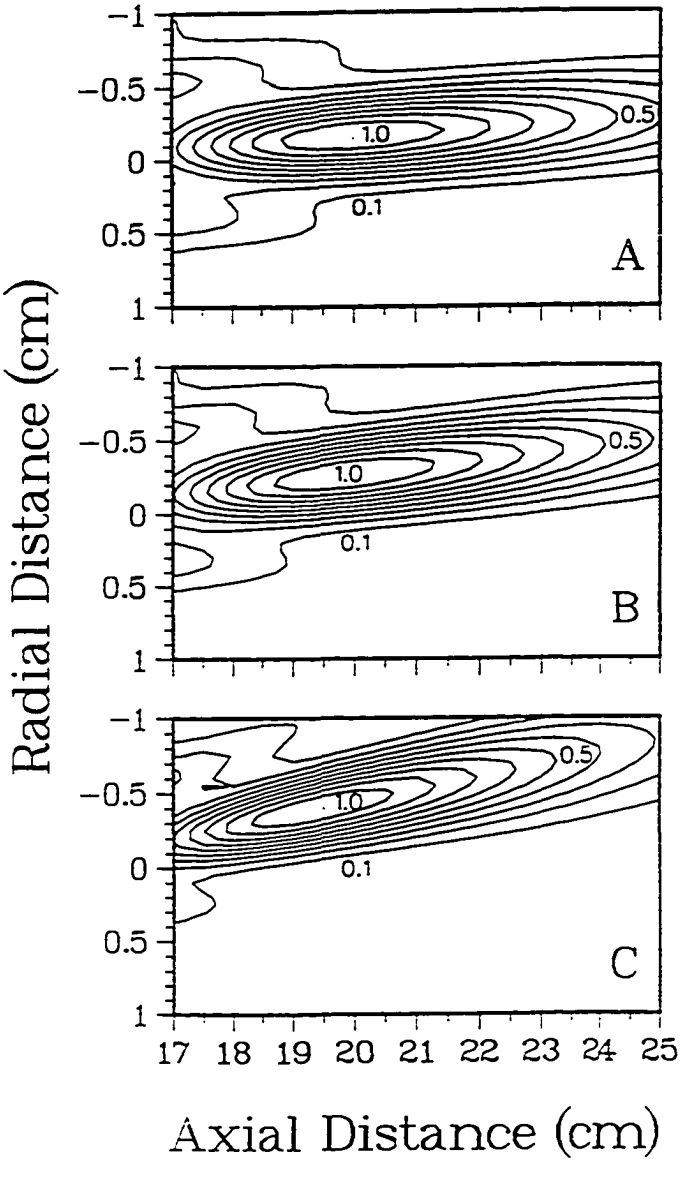

Figure 16. Contour plot of relative pressure amplitude squared for the water-skin-fat-muscle (WSFM) layered model. The transducer had a 25 cm radius of curvature and a 7 cm diameter with a frequency of 1 MHz. The axial distance from the transducer to the skin was 12 cm. The tilted angle of the transducer was: (A) 30°, (B) 45°, (C) 60°.

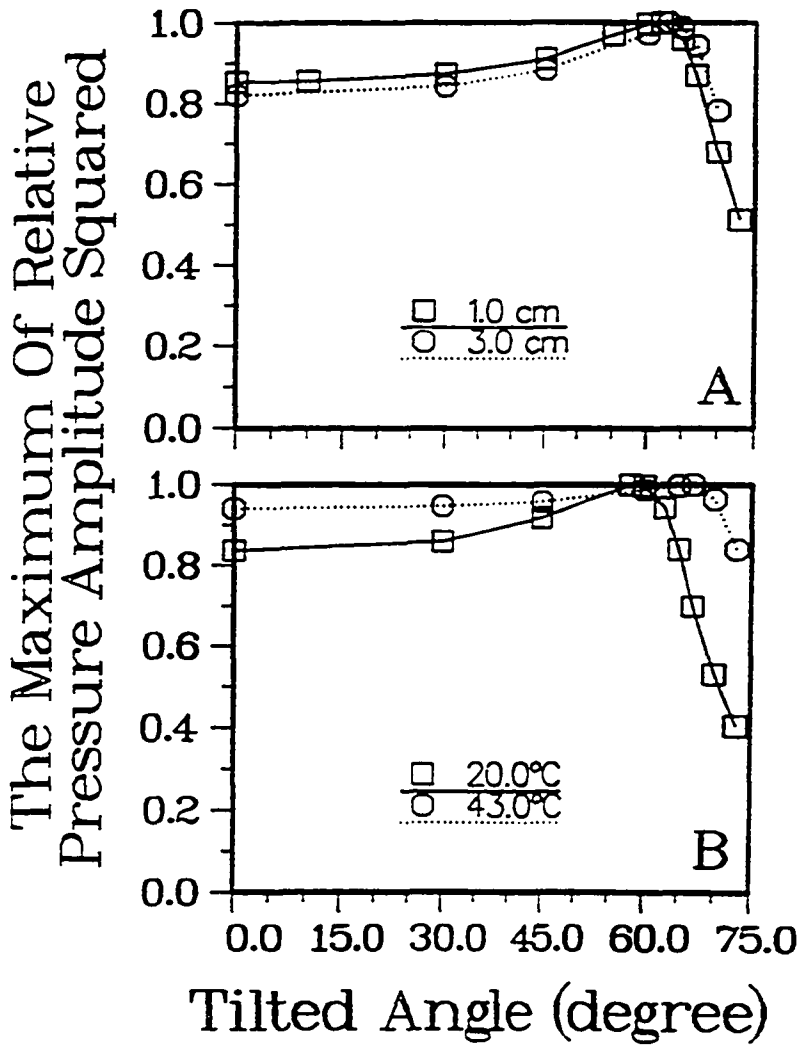

Figure 17. The maximum of the relative pressure amplitude squared response as a function of the angle of the transducer tilted in the WSFM layered model. The transducer had a 25 cm radius of curvature and a 7 cm diameter with a frequency of 1 MHz. (A) variant of fat thickness (water temperature 26.3°C); (B) variant of water temperature (fat thickness 1 cm).

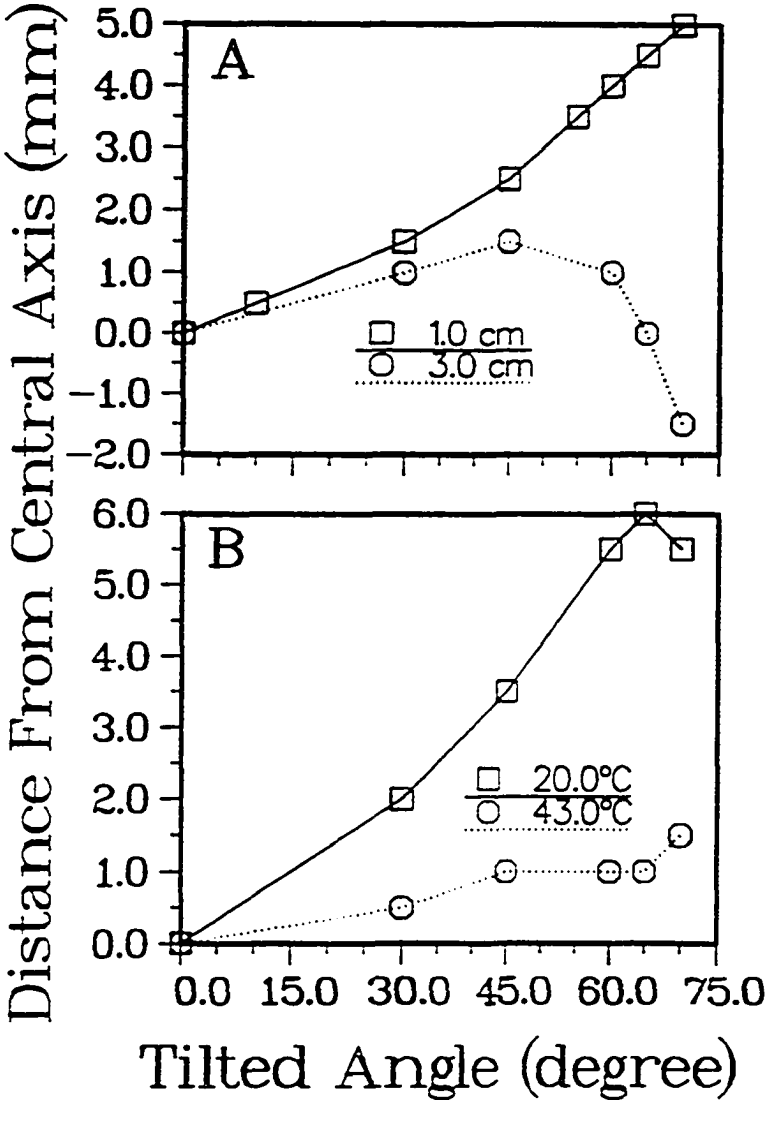

Figure 18. The distance of the maximum pressure of amplitude from the central axis as a function of the transducer tilt angle. All of the conditions are the same as in Figure 17.

4.4 Effect of curved tissue interfaces

In order to study the effect of curved tissue interfaces on power deposition, the irregular interface program was applied to the five models above. The normalized absorbed power depositions as a function of radial distances were studied in the following simulations. For the brain model (Figure 19), four transducer axis locations were studied. The central axial distance from the transducer to the skin was 13 cm when the transducer axis aimed through the center of the sphere. The focus of the beam shifted no more than 3 mm when the transducer central axis was 7 cm away from the center of the sphere. Since the attenuation distances was reduced quadratically as the distance of the central axis to the center of the sphere was increased, the maximum value was increased and dominated the effect of the sound wave reflection and refraction on the tissue interfaces. In Figure 20 the ultrasound field in the axial plane is given. The whole acoustic focus shifted when the transducer axis moved to the edge of the brain.

For the neck model, the axial distance from the transducer to the tissue interface was 13 cm when the transducer axis was aimed through the center of the cylinder (Figure 21). When the transducer central axis was moved 4 cm laterally, the beam focus was shifted up to 2.5 mm and the maximum value was increased slightly. When the transducer central axis was 5 cm away from the center, the maximum value was increased about 25% of the 0 cm case and the beam distorted slightly. For the body and the buttocks models, the beam focus was shifted slightly when the transducer axis was moved away from the center of the geometries (Figure 22 A,B). The amplitude of the power field was increased because the attenuation distances was decreased quadratically.

Finally, the effect of ultrasound wave reflection from bone on the pressure amplitude squared distributions was studied (Figure 23). The standing wave pattern is shown in the calculated field. The amplitude of the standing wave was reduced when the focus of the transducer was moved away from the bone. The magnitude of the acoustic field was large near the tissue-bone interface.

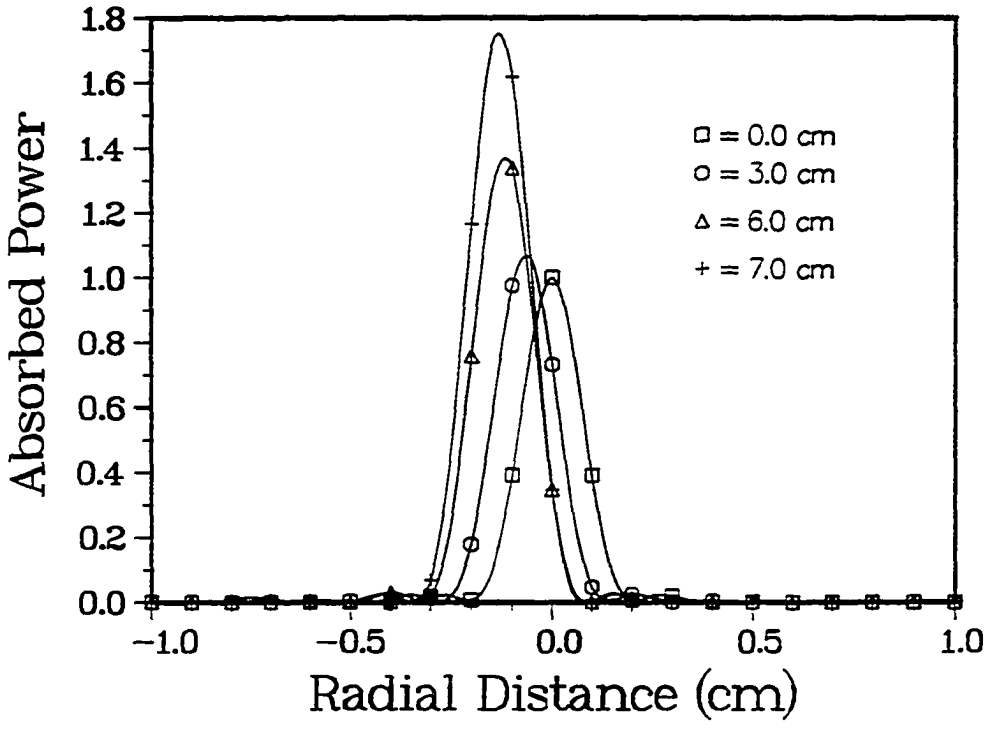

Figure 19. Normalized absorbed power as a function of radial distance for the brain model. The 20 cm radius of curvature and the 10 cm diameter transducer was used with frequencies 1.75 MHz. The central axial distance from the transducer to the tissue interface was 13 cm. The centimeters in the legend indicate the distance from the transducer axis to the center of the brain. The position of the center of the axis of the transducer from the center of the model is given in the Figure 7B.

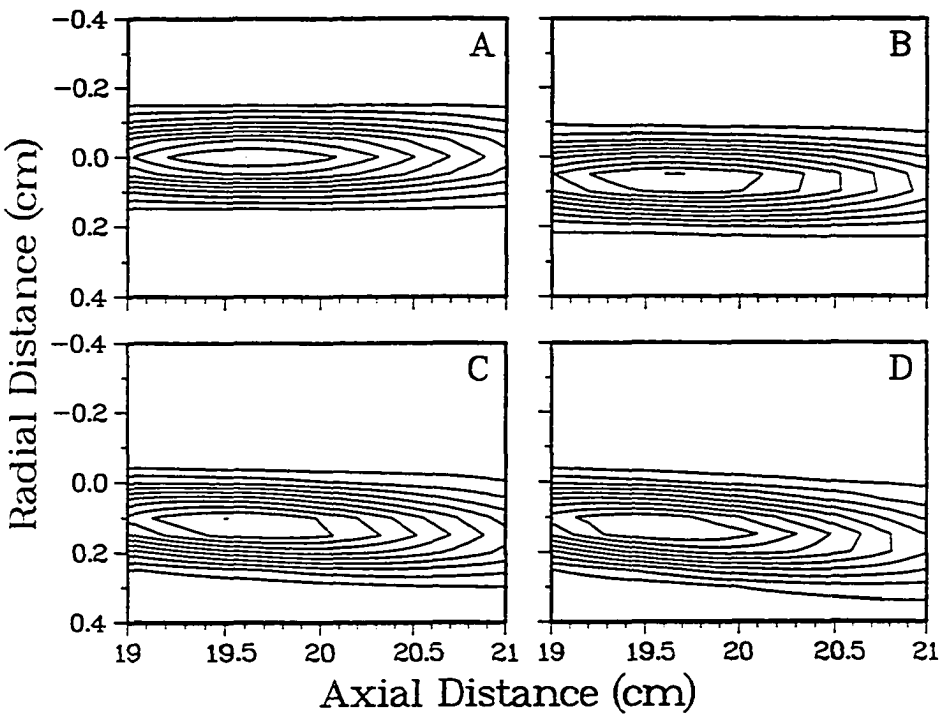

Figure 20. Contour plot of normalized absorbed power for the brain model studied in Figure 19. The distance from the transducer axis to the center of the brain is: (A) 0.0 cm, (B) 3.0 cm, (C) 6.0 cm, (D) 7.0 cm.

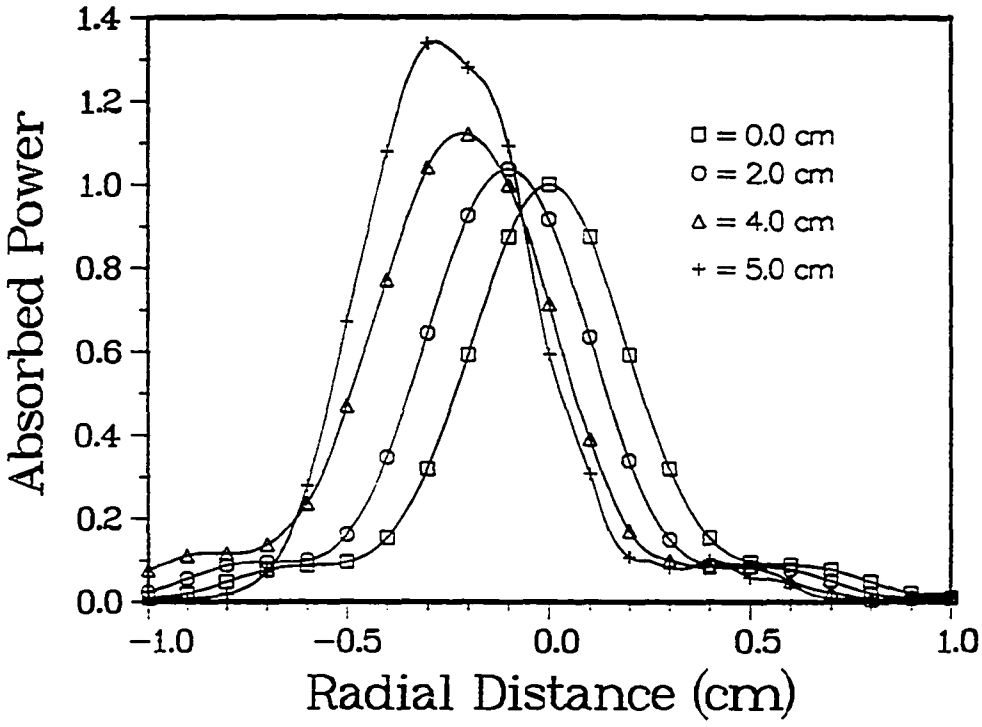

Figure 21. Normalized absorbed power as a function of radial distance for the neck model. The 25 cm radius of curvature and 7 cm diameter transducer was used with a frequency 1 MHz. The central axial distance from the transducer to the tissue interface was 13 cm. The centimeters in the legend indicate the distance from the transducer axis to the center of the neck.

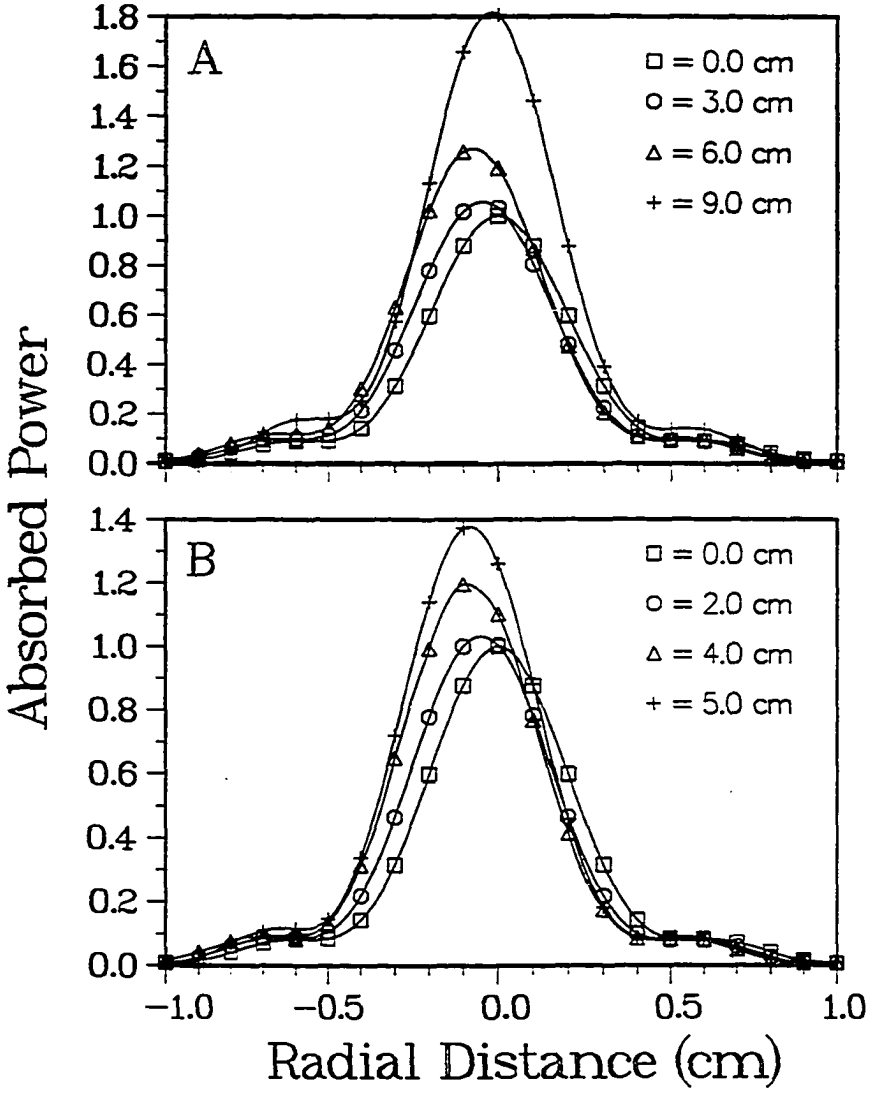

Figure 22. Normalized absorbed power as a function of radial distance for (a) the body and (b) the buttocks models. The 25 cm radius of curvature and 7 cm diameter transducer was used with a frequency of 1 MHz. The central axial distance from the transducer to the tissue interface was 13 cm. The centimeters in the legend indicate the distance from the transducer axis to the center of the body or buttocks.

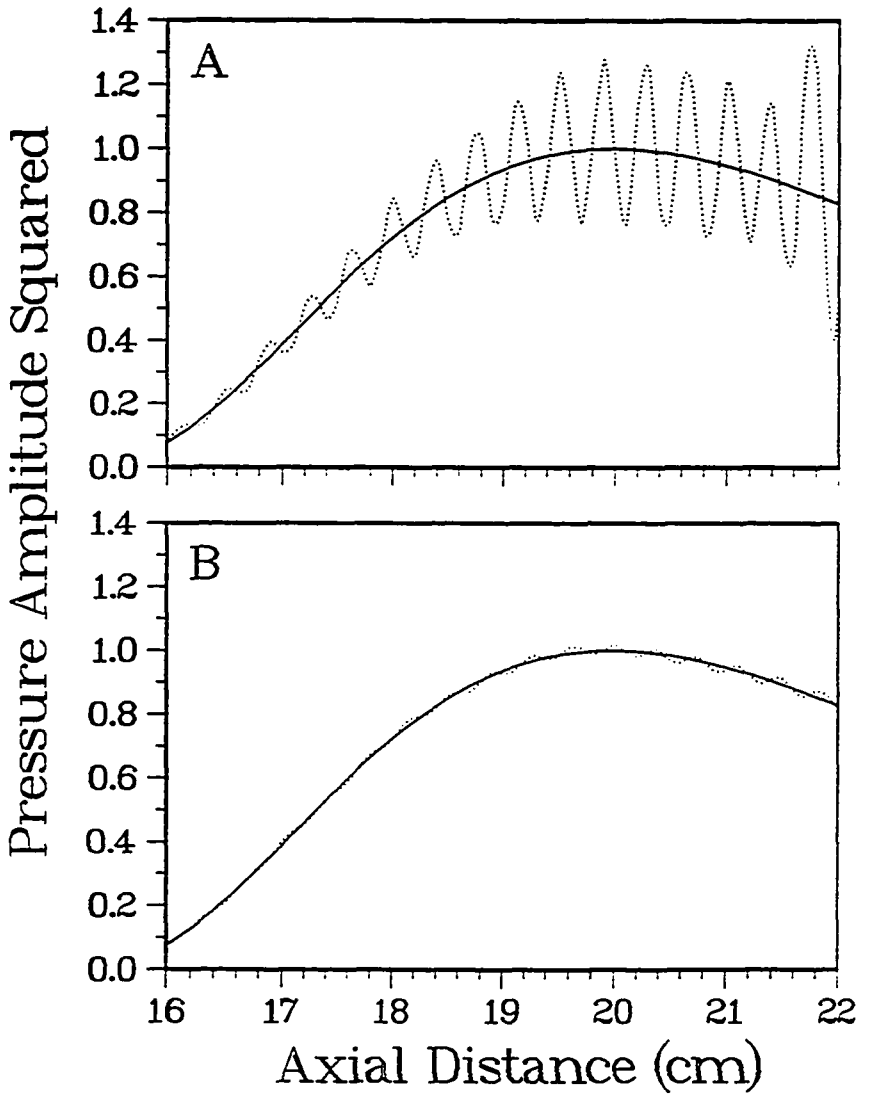

Figure 23. The squared pressure amplitude as a function of axial distance. The 25 cm radius of curvature and 7 cm diameter transducer was used with a frequency of 1 MHz. The tissue interface is at 12 cm. There was a bone, which was a cylinder with radius 1 cm, in the tissue layer along the central axis. The central axis distance from the transducer to the tissue-bone interface was (a) 23.5 cm and (b) 29.5 cm. (—— without bone, ····· with bone)

CHAPTER 5

5. DISCUSSION

When the theoretical model was compared with the experimental results there was good agreement between the simulated and the measured pressure amplitude squared distributions. When the speed of sound differences are very large between media, the theory does not give the correct results because the contributions of a multi wave reflection and refraction are ignored. The contribution from multi reflected wave was estimated to be less than 2% at soft tissue interfaces. When a longitudinal wave travelled through a liquid-solid interface, both a longitudinal and shear wave are generated inside the solid. The shear wave would cause more energy to be reflected at the boundary and more shift of the beam profile for the transducer tilted case. The new model does not consider the shear wave in the calculations because during an ultrasound hyperthermia treatment the propagating waves are mainly longitudinal with the shear waves being generated only under special circumstance (Frizzell and Carstensen 1976; Madsen *el al.* 1983; Chan *et al.* 1974).

The differences between the experiments and the simulations can also be attributed to : (1) a real transducer does not emit power uniformly over its surface; and (2) the surface of the plastic may have not been smooth, causing more energy to be lost at the interface.

Since the beam size is limited for a focused transducer, the size of the secondary wave front was limited too. Usually, the diameter of the tissue interface used in the simulation was less than the diameter of the transducer, especially for strongly focused transducers. In order to get accurate numerical results, the element area of the interface was taken as ten or twenty times less than the wave length squared. For this specific calculation method, the interface size should be larger than the beam width in order to get correct results, otherwise the phases of the particle velocities would not have enough contributions to keep the focus at the right location. When the interface was very curved, the interface should be divided into smaller area elements to reduce the phase error. The calculation time for this irregular interface model proved to be a hundred times larger than the parallel plane interface model.

The interfaces and tissue layers can be ignored for most hyperthermia cases, and thus, the simplified model is adequate for treatment field prediction. This is especially true since random thickness variation would cause less beam shift (Wang *et al.*, 1990) and thus, our calculations are for the worst case situation. The advantage of the simplified model is that the calculation is hundreds of times faster than the double integration method used in this study. This simplified model has also been compared with a real focused ultrasound source and has been found to give a reasonable approximation of the pressure field (Madsen *et al.*, 1981, Moros and Hynynen 1991). The assumption in attenuation distance is good with no large effects on the pressure field except for the small F-number transducer and high frequencies.

The layered tissues will have an impact on the location of the focus when sharply focussed ultrasound beams are used to deliver the treatment during a

high power short duration pulse (Billard *et al.*, 1989,1990, Davis and Lele 1989). Both the location and the acoustic pressure amplitude will be affected enough to bring unacceptable uncertainty in the thermal exposure, unless the tissue layers are accounted for in the model.

The effect of the fat layer on the beam shape can be explained by the speed of sound in the medium. When the wave is propagating from water (high velocity) into the skin-fat layer (low velocity), the refracted wave deviated toward the normal direction. When the fat layer thickness was increased, the distance the refracted wave traveled grew and caused the focus to become longer. When the water temperature was increased, the speed of sound in water became larger than the tissue. This effect caused the refracted wave, which originally deviated away from the normal, to deviate toward the normal. This phenomenon lengthened the focus. In a layered medium, when the flat plane interfaces had an angle with the transducer, the wave would deviate more in one part of the transducer than others, this would cause the focus to become narrower with a larger tilt angle.

There is a critical angle beyond which total reflection will occur when the sound wave travels from the low velocity medium to the high velocity medium, $c_1 < c_2$. The critical angle is given by $\sin^{-1}(c_1/c_2)$ (Chivers and Santosa, 1986). From the simulation results, it is clear that when the transducer is tilted around 60°, complete reflection is reached. For typical values of the speed of sound in fat (1445 m/s) and in muscle (1569 m/s) used during the simulation, the critical angle was 67.1°. This angle agrees well with the simulated results. In most clinical situations the incident angles are small.

When the central axis was moved toward the edge of anatomic geometries, the attenuation distance was reduced quadratically and the maximum amplitude

of the ultrasound field was increased. The effect of attenuation distance dominated the effect of sound wave reflection and refraction because the impedance of the soft tissue was quite close and the beam incident angle was much less than the critical angle for total reflection . There was a beam shift when the central axis of the transducer was away from the center, but the shift distance was smaller for curved interfaces than for the flat plane tissue interface model. The beam shift was larger for the brain and the neck models than for the body and the buttocks models. This is because the radius of curvature of the interfaces for the brain and the neck models were smaller than the other two models. Since the radius of curvatures of the interface were relatively large, the effect of sound wave reflection and refraction was small for these four models. When the transducer axis was aimed near the edge of the anatomical geometry, a beam distortion could happen, especially for weakly focused transducers. Since the acoustic impedances of bone is very much different from the soft tissues, the bone reflects the energy and distorts the beam geometry. This phenomena was agreed with the experimental results given by Lele (1967).

CHAPTER 6

6. CONCLUSIONS

A theoretical computer model that takes reflection and refraction of an ultrasound beam at tissue interfaces into account was developed, tested, and used in this study. The aim was to obtain a quantitative measure of the effect that soft tissue interfaces have during hyperthermia treatments. Generally, the effect of the interfaces was small and it could be ignored during scanned focussed ultrasound hyperthermia treatments where focussed ultrasound beams are scanned to treat the target volume (Lele 1983, 1989, Hynynen *et al.*, 1987, 1990). If the entrance angle of the beam is smaller than 60°, then the beam pattern can be well approximated by the uniform model. The small deviations caused by a fat layer, or water temperature variations will not have a major impact on the temperature distribution. The other uncertainties, such as the location of the tumor boundary (an uncertainty of typically 5-10 mm) and temperature distribution variations caused by blood perfusion (the temperature can be as much as a factor of 5 higher in necrotic tissue than in highly perfused tissue when exposed to the same ultrasound field (Hynynen *et al*, 1990)) are significantly larger than the effect of the soft tissue interfaces observed here.

The new model results give some important information in order to develop an accurate treatment plan in ultrasound hyperthermia. For instance, the theory can predict how large of an angle the transducer can be tilted, how far the beam

profile will be shifted off the central axis, and how much the beam distortion will be; all of which are extremely important for treating small tumors. The ultrasound imaging beams formed by much smaller apertures, are likely to be refracted through the same angle as the therapy beams are reflected. Therefore, ultrasound imaging could be used to locate the target volume and to aim the therapy beams (Hynynen *et al*, 1987). It is important to prevent a bone inside the cone of sound in the ultrasound surgery.

APPENDIX A : Plane Wave Theory

Consider a plane, one dimensional acoustic wave is travelling in two layered medium with the flat plane interface, see Figure 3. The acoustic velocity *potential* for incident, reflected, and transmitted waves is given by

$$\begin{cases} \psi_i(\mathbf{r}) = A_i \exp(i\omega \mathbf{n}_i \cdot \mathbf{r}/c_1) \\ \psi_r(\mathbf{r}) = A_r \exp(i\omega \mathbf{n}_r \cdot \mathbf{r}/c_1) \\ \psi_t(\mathbf{r}) = A_t \exp(i\omega \mathbf{n}_t \cdot \mathbf{r}/c_2) \end{cases} \tag{A.1}$$

where ω is the angular frequency; $\mathbf{n}_i$, $\mathbf{n}_r$, $\mathbf{n}_t$ are unit vectors normal to the direction of wave propagation; A_i, A_r, A_t are the amplitude of the incident, the reflected and the transmitted wave; $\mathbf{r}$ is the two dimensional position vector; c_i is the velocity of sound in medium i, $i = 1, 2$. Notice that the bold face character represents a vector in this appendix. In terms of the coordinate system, unit normal vectors are given by

$$\begin{cases} \mathbf{n}_i = \mathbf{i}\sin(\theta_i) - \mathbf{j}\cos(\theta_i) \\ \mathbf{n}_r = \mathbf{i}\sin(\theta_r) + \mathbf{j}\cos(\theta_r) \\ \mathbf{n}_t = \mathbf{i}\sin(\theta_t) - \mathbf{j}\cos(\theta_t) \end{cases} \tag{A.2}$$

where θ_i, θ_r, θ_t are the incident, the reflected and the transmitted angles referenced to the normal of the interface; $\mathbf{i}$ and $\mathbf{j}$ are unit vectors in the x and the y direction. Since the position vector is $\mathbf{r} = \mathbf{i}x + \mathbf{j}y$, the velocity potential can be written as

$$\begin{cases} \psi_i(x,y) = A_i \exp\left[i\omega \left(x\sin(\theta_i) - y\cos(\theta_i)\right)/c_1\right] \\ \psi_r(x,y) = A_r \exp\left[i\omega \left(x\sin(\theta_r) + y\cos(\theta_r)\right)/c_1\right] \\ \psi_t(x,y) = A_t \exp\left[i\omega \left(x\sin(\theta_t) - y\cos(\theta_t)\right)/c_2\right]. \end{cases} \tag{A.3}$$

Since acoustic pressure $P = \rho\partial\psi/\partial t$ and the velocity $\mathbf{V} = -\nabla\psi$, the pressure and velocities for incident, reflected and transmitted waves are

$$\begin{cases} P_i = -i\omega\rho_1\psi_i \\ P_r = -i\omega\rho_1\psi_r \\ P_t = -i\omega\rho_2\psi_t \end{cases} \tag{A.4}$$

$$\begin{cases} \mathbf{V}_i = i\omega\psi_i\left[-\mathbf{i}\sin(\theta_i) + \mathbf{j}\cos(\theta_i)\right]/c_1 \\ \mathbf{V}_r = i\omega\psi_r\left[-\mathbf{i}\sin(\theta_r) + \mathbf{j}\cos(\theta_r)\right]/c_1 \\ \mathbf{V}_t = i\omega\psi_t\left[-\mathbf{i}\sin(\theta_t) + \mathbf{j}\cos(\theta_t)\right]/c_2 \ . \end{cases} \tag{A.5}$$

The boundary conditions are that the acoustic pressure and the normal component of the velocity are continuous across the interface at $y = 0$, i.e,

$$P_i + P_r = P_t \tag{A.6.a}$$

$$\left[(\mathbf{V}_i + \mathbf{V}_r) - \mathbf{V}_t\right] \cdot \mathbf{j} = 0 \ . \tag{A.6.b}$$

From equation (A.6.b), the following relation can be obtained,

$$\frac{\cos(\theta_i)}{c_1} A_i \exp\left(i\omega\frac{x}{c_1}\sin(\theta_i)\right) - \frac{\cos(\theta_r)}{c_1} A_r \exp\left(i\omega\frac{x}{c_1}\sin(\theta_r)\right) - \frac{\cos(\theta_t)}{c_2} A_t \exp\left(i\omega\frac{x}{c_2}\sin(\theta_t)\right) = 0. \tag{A.7}$$

Equation (A.7) must hold for any value of x, therefore the following two equalities can be obtained

$$\sin(\theta_i)/c_1 = \sin(\theta_r)/c_1 = \sin(\theta_t)/c_2 \tag{A.8}$$

which leads to

$$\theta_i = \theta_r, \quad \text{and} \quad c_2\sin(\theta_i) = c_1\sin(\theta_t). \tag{A.9}$$

Applying these results to the boundary condition for the velocity (equation (A.6.b)) yields

$$\cos(\theta_1)(A_i - A_r)/c_1 = \cos(\theta_2)A_t/c_2 \ . \qquad (A.10)$$

Here the notation for θ was changed to $\theta_i \rightarrow \theta_1$, $\theta_t \rightarrow \theta_2$. Similarly, the boundary condition for the pressure, given by equation (A.6.a) becomes

$$\rho_1(A_i + A_r) = \rho_2 A_t. \qquad (A.11)$$

Solving the system of equations (A.10) and (A.11), the equations for the amplitudes of A_r and A_t in terms of A_i are

$$A_t = \frac{2\rho_1 c_2 \cos(\theta_1)}{\rho_2 c_2 \cos(\theta_1) + \rho_1 c_1 \cos(\theta_2)} A_i \qquad (A.12)$$

$$A_r = \frac{\rho_2 c_2 \cos(\theta_1) - \rho_1 c_1 \cos(\theta_2)}{\rho_2 c_2 \cos(\theta_1) + \rho_1 c_1 \cos(\theta_2)} A_i. \qquad (A.13)$$

The acoustic pressure amplitudes for the incident, the reflected and the transmitted waves from equation (A.4) are

$$A_i^p = \omega\rho_1 A_i, \quad A_r^p = \omega\rho_1 A_r, \quad A_t^p = \omega\rho_2 A_t \ . \qquad (A.14)$$

Using equation (A.12), the acoustic pressure transmission coefficient is

$$T_p = \frac{A_t^p}{A_i^p} = \frac{2Z_2 \cos(\theta_1)}{Z_2 \cos(\theta_1) + Z_1 \cos(\theta_2)}, \qquad (A.15)$$

where $Z_i = \rho_i c_i$ is the acoustic impedance in medium i, $i = 1, 2$. From equation (A.5), the amplitudes of the velocities for the incident, the reflected, and the transmitted waves are

$$A_i^v = \omega A_i/c_1, \quad A_r^v = \omega A_r/c_1, \quad A_t^v = \omega A_t/c_2. \qquad (A.16)$$

Finally, the velocity transmission coefficient is

$$T_v = \frac{A_t^v}{A_i^v} = \frac{2Z_1 \cos(\theta_1)}{Z_2 \cos(\theta_1) + Z_1 \cos(\theta_2)} \tag{A.17}$$

and the velocity reflection coefficient is

$$R_v = \frac{A_r^v}{A_i^v} = \frac{Z_2 \cos(\theta_1) - Z_1 \cos(\theta_2)}{Z_2 \cos(\theta_1) + Z_1 \cos(\theta_2)} \ . \tag{A.18}$$

APPENDIX B : Amplitude Diminution Factor

Differentiating equation C.1 (see Appendix C) produces the following relation

$$\delta\theta_j = \frac{c_j \cos(\theta_1)}{c_1 \cos(\theta_j)}\delta\theta_1, \quad j = 2, \cdots, N.$$

Differentiating equation C.2 (see Appendix C) and applying the above relation yields

$$\delta W = \frac{\cos(\theta_1)}{c_1}\left[\sum_{j=1}^{N} H_j \sec^2(\theta_j)\frac{c_j}{\cos(\theta_j)}\right]\delta\theta_1.$$

Since $W_1 = H_1 \tan(\theta_1)$, its differential is $\delta W_1 = H_1 \sec^2(\theta_1)\delta\theta_1$. The amplitude diminution factor, $A(\theta_1)$, is obtained by combining the above relations.

$$A(\theta_1) = \left[\frac{W_1 \delta W_1}{W \delta W}\right]^{1/2}$$

$$= \left[\frac{H_1^2 \tan(\theta_1)\sec^2(\theta_1)\delta\theta_1}{\frac{\cos(\theta_1)}{c_1}\left(\sum_{j=1}^{N} H_j \tan(\theta_j)\right)\left(\sum_{j=1}^{N} H_j \sec^2(\theta_j)\frac{c_j}{\cos(\theta_j)}\right)\delta\theta_1}\right]^{1/2}$$

This equation can be rewritten as

$$A(\theta_j) = \frac{H_1}{\left[H_1 + \sum_{j=2}^{N}\frac{c_j H_j}{\cos(\theta_j)}\right]^{1/2}\left[H_1 + \sum_{j=2}^{N} c_j H_j \cos^3(\theta_j)\right]^{1/2}},$$

where the following relation has been used

$$\frac{\tan(\theta_j)}{\tan(\theta_1)} = \frac{c_j \cos(\theta_1)}{c_1 \cos(\theta_j)}.$$

APPENDIX C : Newton-Raphson Method

C.1 Equation for finding ray trace

For given point sources in an N layered medium with parallel plane interfaces, the ray trace of the acoustic wave can be found in terms of the velocity of sound c_i and the thickness of the layers H_i, $i = 1, \cdots, N$. According to Snell's law, the following system equations can be obtained

$$c_i \sin(\theta_{i+1}) = c_{i+1} \sin(\theta_i), \quad i = 1, \cdots, N-1, \tag{C.1}$$

where θ_i is the angle of incidence in medium i and c_i is the velocity of sound in medium i. In order to solve θ_i uniquely, one more equation is needed

$$W = \sum_{i=1}^{N} H_i \tan(\theta_i), \tag{C.2}$$

where W is the distance in the X-axis direction between the point source and the field point of interest.

The Newton-Raphson numerical method (Press *et al.*, 1989), was used to solve the nonlinear system of equations given by equation (C.1) and (C.2). Define the following functions by using the relation $\sin(\theta_i) = X_i / \sqrt{H_i^2 + X_i^2}$

$$\begin{cases} f_i(X_1, X_2, \cdots, X_N) = c_i \frac{X_{i+1}}{\sqrt{H_{i+1}^2 + X_{i+1}^2}} - c_{i+1} \frac{X_i}{\sqrt{H_i^2 + X_i^2}}, & i = 1, \cdots, N-1, \\ f_N(X_1, X_2, \cdots, X_N) = X_1 + X_2 + \cdots + X_n - W \end{cases} \tag{C.3}$$

then the matrix equation

$$\sum_{j=1}^{N} \alpha_{i,j} \delta X_j = \beta_i \qquad (C.4)$$

can be solved by LU decomposition (Press *et al.*, 1989), where

$$\alpha_{ij} = \partial f_i / \partial X_j, \quad \beta_i = -f_i. \qquad (C.5)$$

X_i is obtained by the following iteration procedure.

$$X_i^{new} = X_i^{old} + \delta X_i, \quad i = 1, \cdots, N \qquad (C.6)$$

The iteration continues until δX_i is less than a given tolerance. Finally, the incident angle θ_i is obtained from X_i.

C.2 Method for solving the matrix equation

The matrix in equation (C.4) has the following form (assume it's $N \times N$)

$$A = \begin{pmatrix} a_{11} & a_{12} & 0 & \dots & \dots & 0 \\ 0 & a_{22} & a_{23} & 0 & \dots & 0 \\ \vdots & \vdots & \ddots & \ddots & \vdots & \vdots \\ \vdots & \vdots & \vdots & \ddots & \ddots & \vdots \\ 0 & \dots & \dots & 0 & a_{N-1N-1} & a_{N-1N} \\ 1 & \dots & \dots & \dots & 1 & 1 \end{pmatrix}$$

The matrix A is sparse and almost triangular. In order to save computation time, a simplified Gaussian elimination technique is used to solve the linear system of equations $AX = B$. Note that only the last row needs to be row reduced, i.e., all entries in the last row are zeroed except for the NN entry. Consequently, only the last row in the column matrix B will change, i.e.

$$B_N^{new} = B_N^{old} - L_{N1}B_1/a_{11} - L_{N2}B_2/a_{22} - \cdots - L_{NN-1}B_{N-1}/a_{N-1N-1},$$

where

$$\begin{cases} L_{N1} = 1 \\ L_{N2} = 1 - L_{N1}a_{12}/a_{11} \\ \cdots\cdots\cdots\cdots\cdots\cdots \\ L_{NN-1} = 1 - L_{NN-2}a_{N-2N-1}/a_{N-2N-2} \end{cases} .$$

After some algebra, the matrix A can be manipulated into an upper triangular matrix, with the same element values as the original A matrix elements, except for the following changes in the last row. All entries in the last row become zero except for the NN entry which becomes

$$a_{NN} = 1 - L_{NN-1}a_{N-1N}/a_{N-1N-1} \ .$$

The value for X can be obtained by back substitution.

APPENDIX D : Distances

D.1 Distance from a point to a plane

The distance d from a point (x_0, y_0, z_0) to a plane $Ax + By + Cz + D = 0$ is given by

$$d = \frac{|Ax_0 + By_0 + Cz_0 + D|}{\sqrt{A^2 + B^2 + C^2}}, \tag{D.1}$$

where (A, B, C) is the normal direction of the plane.

D.2 Distance W along a plane between two points separated by the plane

Consider two points (X_i, Y_i, Z_i), $i = 1, 2$ separated by a plane (Figure D.1). From each point draw a line perpendicular to the plane and denote the intersection points on the plane as (x_i, y_i, z_i), $i = 1, 2$. The distance between these two points needs to be found. Assume the plane equation is

$$Ax + By + Cz + D = 0. \tag{D.2}$$

The two line equations can be written as

$$\frac{x_i - X_i}{A} = \frac{y_i - Y_i}{B} = \frac{z_i - Z_i}{C} = t_i, \quad i = 1, 2, \tag{D.3}$$

where the lines are in the direction of (A, B, C) and t_i is a parameter. From equation (D.3) the following relation can be obtained

$$\begin{cases} x_i = X_i + At_i \\ y_i = Y_i + Bt_i \\ z_i = Z_i + Ct_i \ . \end{cases} \tag{D.4}$$

Since (x_i, y_i, z_i) is on the plane, it must satisfy equation (D.2). Substitute equation (D.4) into equation (D.2), and solve for t_i,

$$t_i = -\frac{AX_i + BY_i + CZ_i + D}{A^2 + B^2 + C^2}.$$

The distance between these two points is given by

$$\begin{aligned} W &= \sqrt{(x_1 - x_2)^2 + (y_1 - y_2)^2 + (z_1 - z_2)^2} \\ &= \sqrt{X^2 + Y^2 + Z^2 - \frac{(AX + BY + CZ)^2}{A^2 + B^2 + C^2}}, \end{aligned}$$

where $X = X_1 - X_2$, $Y = Y_1 - Y_2$, and $Z = Z_1 - Z_2$.

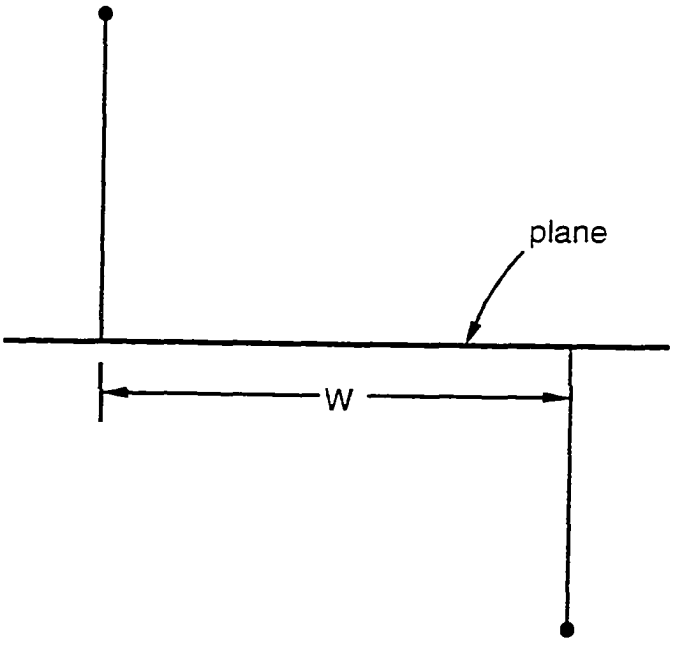

Figure D.1. Two points separated by the plane.

REFERENCES

[1] AIUM (The American Institute of Ultrasound in Medicine).(1988). "Bioeffects considerations for the safety of diagnostic ultrasound," J. Ultrasound Med., vol. 7, No. 9, S1-S38.

[2] Bamber, J.C., and Hill, C.R.(1979). "Ultrasonic attenuation and propagation speed in mammalian tissues as a function of temperature," Ultrasound Med., Biol., vol. 5, pp. 149-157.

[3] Billard, B.E., Hynynen, K., and Roemer, R.B.(1990). "Effects of physical parameters on high temperature ultrasound hyperthermia," Ultrasound Med. Biol., vol. 16, pp. 409-420.

[4] Billard, B.E., Hynynen, K., and Roemer, R.B.(1989). "Introduction of perfusion independent thermal exposure," in Hyperthermic Oncology 1988, vol. 1, eds. T. Sugahara and M. Saito, Taylor & Francis, London, New York, Philadelphia, pp. 713-714.

[5] Cain, C.A., and Umemura, S.-A.(1986). "Concentric-ring and sector vortex phased array applicators for ultrasound hyperthermia therapy," IEEE Trans. Microwave Theory and Techniq., vol. 34, pp. 542-551.

[6] Chan, A.K., Sigelmann, R.A., and Guy, A.W.(1974). "Calculations of therapeutic heat generated by ultrasound in fat-muscle-bone layers," IEEE Trans. Biomed. Eng., vol. 21, pp. 280-284.

[7] Chivers, R.C., and Parry, R.J.(1978). "Ultrasonic velocity and attenuation in mammalian tissues," J. Acoust. Soc. Am., vol. 63, pp. 940-953.

[8] Chivers, R.C., and Santosa, F.(1986). "Numerical considerations for interface reflection in medical ultrasound," Phys. Med. Biol., Vol. 31, No. 8, pp. 819-837.

[9] Davis, B.J., and Lele, P.P.(1989). "A theoretical study of rapid hyperthermia by scanned focussed ultrasound," presented at the Winter Annual Meeting of ASME, San Francisco, CA, December 10-15.

[10] Diederich, C., and Hynynen, K.(1989). "Induction of hyperthermia using an intracavitary multi-element ultrasonic applicator," IEEE Trans. Biomed. Eng., vol. 36, pp. 432-438.

[11] Diederich, C., and Hynynen, K.(1990). "The development of intracavitary ultrasonic applicators for hyperthermia: A design and experimental study," Medical Physics, vol. 17, pp. 626-634

[12] Del Grosso, V.A., and Mader, C.W.(1972). "Speed of sound in pure water," J. Acoust. Soc. Am., vol. 52, pp. 1442-1446.

[13] Frizzell, L.A., and Carstensen, E.(1976). "Shear properties of mammalian tissues at low megahertz frequencies," J. Acoust. Soc. Am., vol. 60, pp. 1409-1411.

[14] Fry, W.J., and Dunn, F.(1962). "Ultrasoumd: Analysis and experimental methods in biological research," in Physical techniques in biological research. Vol. 4, Special methods. ed. W.M. Nastuk, Academic Press, New York, pp. 261-325.

[15] Goss, S.A., Frizzell, L.A., and Dunn, F.(1979). "Ultrasonic absorption and attenuation of high frequency sound in mammalian tissues," Ultrasound Med. Biol., vol. 5, pp. 181-186.

[16] Goss, S.A., Johnson, R.L., and Dunn, F.(1978). "Comprehensive compilation of empirical ultrasonic properties of mammalian tissues," J. Acoust. Soc. Am., vol. 64, pp. 423-457.

[17] Goss, S.A., Johnson, R.L., and Dunn, F.(1980). "Compilation of empirical ultrasonic properties of mammalian tissues," II. J. Acoust. Soc. Am., vol. 68, pp. 93-108.

[18] Hudimac, A.A.(1957). "Ray theory solution for the sound intensity in water due to a point source above it," J. Acoust. Soc. Am., vol. 29, pp. 916-917.

[19] Hynynen, K., Watmough, D.J., and Mallard, J.R.(1981). "Design of ultrasonic transducers for local hyperthermia," Ultrasound Med. Biol., vol. 7, pp. 397-402.

[20] Hynynen, K., Roemer, R., Anhalt, D., Johnson, C., Xu, Z.X., Swindell, W., and Cetas, T.C.(1987). "A scanned, focussed, multiple transducer ultrasonic system for localized hyperthermia treatments," Int. J. Hyperthermia., vol. 3, pp. 21-35.

[21] Hynynen, K., Shimm, D., Anhalt, D., Stea, B., Sykes, H., Cassady, J.R., and Roemer, R.B.(1990). "Temperature distributions during clinical scanned, focussed ultrasound hyperthermia treatments," Int. J. Hyperthermia, vol. 6, pp. 891-908.

[22] Lele, P.P.(1967). "Production od deef focal lesions by focused ultrasound-current status," Ultrasonics, vol. 5, pp. 105-112.

[23] Lele, P.P.(1983). "Physical aspects and clinical studies with ultrasound hyperthermia," In: Storm FC (ed) Hyperthermia in cancer therapy. Hall Medical, Boston, pp. 333-367.

[24] Lele, P.P., Goddard, J., and Blanter, M.(1989). "Thermometric and clinical results of MIT SIMFU (Scanned, Focussed Intensity-Modulated Ultrasound)," in Hyperthermic Oncology 1988, vol. 1, eds. T. Sugahara and M. Saito, Taylor & Francis, London, New York, Philadelphia, vol. 1, pp. 614-716.

[25] Lele, P.P., and Parker, K.J.(1982). "Temperature distributions in tissues during local hyperthermia by stationary or steered beams of unfocussed or focussed ultrasound," Brit. J. Cancer, Suppl. V 45, pp. 108-121.

[26] Lin, W.L., Roemer, R.B., and Hynynen, K.(1990). "Theoretical and experimental evaluation of a temperature controller for scanned focussed ultrasound hyperthermia," Medical Physics, vol. 17, pp. 615-625.

[27] Lyons, M., and Parker, K.J.(1988). "Absorption and attenuation in soft tissues II - Experimental results," IEEE Trans. Ultrason. Ferroldectr. Freq. Control., vol. 35, pp. 511-521.

[28] Madsen, E.L., Goodsitt, M.M., and Zagzebski, J.A.(1981), "Continuous wave generated by focussed radiators," J. Acoust. Soc. Am., vol. 70, pp. 1508-1517.

[29] Madsen, E.L., Sathoff, H.J., and Zagzebski, J.A.(1983). "Ultrasonic shear wave properties of soft tissues and tissuelike materials," J. Acoust. Soc. Am., vol. 74, pp. 1346-1355.

[30] Martin, C.J., and Law, A.N.R.(1983). "Design of thermistor probes for measurement of ultrasound intensity distributions," Ultrasonics., vol. 21, pp. 85-90.

[31] Moros, E.G., Roemer, R.B., and Hynynen, K.(1988). "Simulations of scanned focussed ultrasound hyperthermia: the effect of scanning speed and pattern," IEEE Trans. Ultrason. Ferroelectr. Freq Control., vol. 35, pp. 552-560.

[32] Moros, E.G., and Hynynen, K.(1992). "A comparison of theoretical and experimental ultrasound field distributions in canine muscle tissue in vivo," Ultrasound Med. Biol., vol. 18, No. 1.

[33] Moros, E.G., Roemer, R.B., and Hynynen, K.(1990). "Pre-focal plane high temperature regions induced by scanning focussed ultrasound beams," Int. J. Hyperthermia, vol. 6, pp. 351-366.

[34] Nyborg, W.L.(1981). "Heat generation by ultrasound in a relaxing medium," J. Acoust. Soc. Am., vol. 70, pp. 310-312.

[35] O'Neil, H.T.(1949). "Theory of focussing radiators," J. Acoust. Soc. Am., vol. 21, pp. 516-526.

[36] Press, W.H., Flannery, B.P., Teukolsky, S.A. and Vetterling, W.T. (1989) Numerical Recipes. Cambridge University Press.

[37] Roemer, R.B., Swindell, W., Clegg, S.T., and Kress, R.L.(1984). "Simulation of focussed, scanned ultrasound heating of deep-seated tumors: the effect of blood perfusion," IEEE Trans. Sonics Ultrasound, vol. 31, pp. 457-466.

[38] Ristic, V.M. (1983) Principles of Acoustic Devices. A Wiley-Interscience Publication, John Wiley & Sons, Inc.

[39] Stewart, H. F.(1982). "Ultrasonic measurement techniques and equipment output levels," In: Repacholi MH, Benwell DA (eds) Essentials of medical ultrasound. Humana, Clifton, NJ, pp. 77-116.

[40] Swindell, W., Roemer, R.B., and Clegg, S.T.(1982)."Temperature distributions caused by dynamic scanning of focussed ultrasound transducers," Proc. IEEE/SU Ultrason. Symp. (IEEE No.0090-5607), pp. 745-749.

[41] Urick, R.J.(1972). "Noise signature of an aircraft in level flight over a hydrophone in the sea," J. Acoust. Soc. Am., vol. 52, pp. 993-999.

[42] Wang, H., Ebbini, E., and Cain, C.(1990). "Effect of phase errors on field patterns generated by an ultrasound phased array hyperthermia applicator," IEEE Trans. Ultrasonics, Ferroelectrics, and Frequency Control, vol. 38, pp. 521-531.

[43] Wells, P.N.T.(1977). Biomedical Ultrasonics. Academic Press, London.

[44] Young, R.W.(1973). "Sound pressure in water from a source in air and vice versa," J. Acoust. Soc. Am., vol. 35, pp. 1708-1716.

[45] Zemanek, J.(1971). "Beam behavior within the nearfield of a vibrating piston," J. Acoust. Soc. Am., vol. 49, pp. 181-191.